INVESTIGATION OF INTERACTION ENERGIES OF TOPOISOMERASE I INHIBITOR: TOPOTECAN

by

Ayşe Kumru Dikmenli

B.S., Chemistry, Boğaziçi University, 2014

Submitted to the Institute for Graduate Studies in
Science and Engineering in partial fulfillment of
the requirements for the degree of
Master of Science

Graduate Program in Chemistry

Boğaziçi University

2015

To my family

ACKNOWLEDGEMENTS

I wish to express my deepest gratitude to my advisors Prof. Viktorya Aviyente and Assist. Prof. Saron Catak for giving me the opportunity to work on this project. They inspired me with their profound guidance.

I would like to thank the members of the examining committee, Prof. İlknur Doğan, Assist. Prof. Oktay Demircan and Assoc. Prof. Nurcan Tüzün for their contribution and advice.

I would also like to thank the members of Aviyente lab, Tuğba, Burcu, Sesil, Gülşah for their scientific insight and unending patience.

I would like to express how lucky I find myself to be friends with Neşe and İdil, for accepting me at my best and worst. Also, my friends from the Department especially Buğra, Tuğçe, Furkan, Dilara and İrem. I am indebted to all of my dear professors from the Bogazici University for teaching me not just chemistry but also how to be a better person.

I thank my family, for their unwavering support and respect, I am proud to be their daughter.

This research has been financially supported by TUBITAK and BAP.

ABSTRACT

INVESTIGATION OF INTERACTION ENERGIES OF TOPOISOMERASE I INHIBITOR: TOPOTECAN

Topoisomerases (Top1) cut one or both strands of DNA and therefore bring changes in the topology of DNA. They are ubiquitous enzymes which are essential for the cellular regulation of DNA supercoiling caused by processes such as replication, transcription, and recombination. These enzymes also adjust the steady state level of DNA supercoiling in order to facilitate protein-DNA interactions. Because of their crucial roles in DNA replication, topoisomerases are the focus of many cancer research, as they are the sole target for several families of anti-cancer drugs that are typically medium size organic molecules. The drug chosen for this project is Topotecan (TPT) which belongs to Camptothecin (CPT) family of anticancer drugs. The main purpose of this research is the application of three major physical theories on mechanics, namely quantum, classical, and statistical, in a harmonious blend to focus on different aspects of the dynamic mechanism of the DNA-Topoisomerase and DNA-Topoisomerase-TPT molecular systems. The large scale atomistic studies have been conducted by Levent Sarı from Fatih University, they have been coupled with the electronic level calculations in this study. Quantum chemical methods used in this study are DFT and semi-empirical theory. Overall, in this project, we aimed to combine both electronic level static calculations (quantum chemical data based on the time-independent Schrödinger equation) and time dependent data obtained at the atomic level (molecular dynamical calculations), and have used them together to gain deeper understanding on Top1-TPT-DNA interactions.

ÖZET

TOPOİZOMERAZ I İNHİBİTÖRÜ TOPOTECANIN ETKİLEŞİM ENERJİLERİNİN İNCELENMESİ

Topoisomerazlar (Top1) DNA nın bir veya iki zincirini keserek DNA nın replikasyon esnasında topolojisinin düzenlenmesi ve kromozomların ayrılması gibi çok önemli hücresel faaliyetlerde bulunurlar. Bu yüzden replikasyon, transkripsiyon ve rekombinasyon gibi temel hücresel aktivitelerde DNA'nın değişen topolojisini (özellikle süperkoil seviyesini) ayarlama görevi topoisomeraz proteinleri tarafından yapılır. DNA'nın superkoil seviyesinin belirli bir seviyede tutulması, diğer hücresel fonksiyonları iş yapan proteinlerle olan ilişkisinin düzenli olması noktasında ve hücre içeresinde kompakt bir şekilde yerleşebilmesi için oldukça önem arz etmektedir. Özellikle DNA'nın replikasyonunda, Top1 proteinlerinin aktif rol oynaması, bu proteinlerin bir çok kanser araştırmasında odak haline gelmesine sebep olmuştur. Bu araştırma için seçilen kanser ilacı Camptothecin sınıfından Topotecan (TPT) ilacı olmuştur. Bu projenin temel amacı, fizikte mekanik üzerine kurulu üç temel teori olan, kuantum, klasik, ve istatiksel mekanik teorilerini birbirleri ile uyumlu bir şekilde kullanarak, DNA-Top1-TPT sistemini değişik seviyelerde incelemektir. Binlerce atomdan oluşan bu büyük ölçekteki dinamik hesaplar Fatih Üniversitesi'nden Levent Sarı tarafından yapılmıştır. Bu projede ise Top1 aktivitesini hedef alan orta büyüklükteki kuvantum mekaniksel hesaplar ile birleştirilmiştir. Elektronik seviyedeki teorik hesaplamalarda DFT ve semi-emprik yöntemler kullanılmıştır. Kısaca, bu projede, elektronik seviyedeki statik hesaplar (zamandan bağımsız Schrödinger denklemi üzerine kurulu kuvantum mekaniksel hesaplar) ile atomik seviyede zamana bağlı hesapları (klasik ve istatiksel mekanik üzerine kurulu moleküler dinamiksel hesapları) biraraya getirip, Top1-TPT-DNA etkileşimleri üzerine yeni bilgilere ulaşılması hedeflenmiştir..

TABLE OF CONTENTS

LIST OF TABLES

LIST OF FIGURES

LIST OF ACRONYMS/ABBREVIATIONS

Asn	Asparagine
Asp	Aspartate
CPT	Campthothecin
DNA	Deoxyribonucleic acid
DFT	Density functional theory
Ec[ρ]	Correlation energy
ΔE_{INT}	Interaction energy
$E_X[\rho]$	Exchange energy
$E_{XC}[\rho]$	Exchange-correlation energy
HF	Hartree–Fock
His	Histidine
J[ρ]	Coulomb energy
Lys	Lysine
MD	Molecular dynamics
ρ(r)	Electron density
Thr	Threonine
Top1	Topoisomerase 1
Top1cc	Cleavage complex
T[ρ]	Kinetic energy of interacting electrons
TPT	Topotecan
Ts[ρ]	Kinetic energy of non-interacting electron
Tyr	Tyrosine
$V[\rho(r)]$	Electron-electron interaction
Ψ	Many electron wavefunction

1. INTRODUCTION

1.1. Topoisomerase

Essential cellular processes such as replication, transcription, chromatin assembly, recombination, and chromosome segregation require unwinding of double stranded structure of DNA. Rapid unwinding results in topological distortions in DNA, also called supercoils, can prevent essential DNA metabolism. Such supercoiling can be relaxed by one of the ubiquitous nuclear enzymes Topoisomerase 1 (Top1). The crystal structure first unraveled in the 70's [1-5], Top1 targets double stranded DNA and single stranded DNA in case of a hairpin loop [6]. Human Top1 in Figure 1.1 consists of 785 amino acid residues, from 4 domains namely: core domain with 420 residues, C-terminal domain with 52 residues, N-terminal domain with 214 residues and linker domain with 76 residues [7].

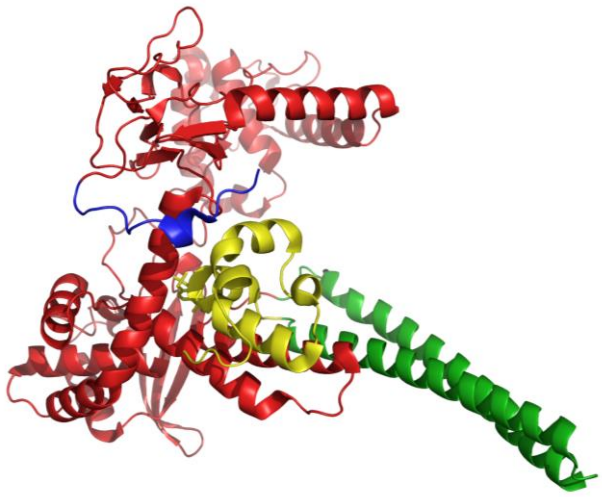

Figure 1.1. Domain structure of human Top1. Domains of the protein are shown with the following color schemes: red, core domain; yellow, C-terminal domain; green, linker domain and blue, N-terminal domain.

The crystal structure of human Top1 was discovered in 1998 and the mechanism of action resolving DNA supercoils was explained in several steps [8]: (i) the enzyme surrounds DNA to form a non-covalent Top1-DNA complex which is stabilized by hydrogen bonds and electrostatic interactions. (ii) Covalent complex is established via nucleophilic attack of

the hydroxyl group of catalytic tyrosine (Tyr723 in C-terminal) on a DNA phosphodiester bond, resulting in cleaved DNA backbone as illustrated in Figure 1.2. (3) After the cleavage, the proposed "controlled rotation" mechanism in Figure 1.3, occurs as the 5′-OH broken strand rotates around the unbroken strand to relax torsional stress in DNA [9]. (4) Resulting covalent phosphotyrosine intermediate, also known as "cleavable complex", at the 3′ end religates when attacked by the free hydroxyl group on 5′ end of the broken DNA strand through an esterification to religate the phosphodiester backbone of DNA and release the enzyme [2].

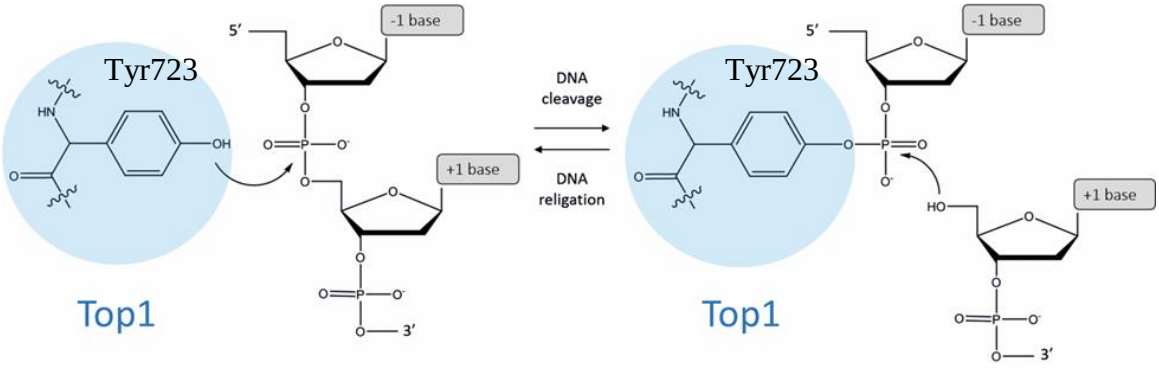

Figure 1.2. Topoisomerase mediated DNA cleavage and religation mechanisms.

Under normal conditions, cleavage complex is unstable and religation is preferred [10]. But before the religation, the complex is highly vulnerable to inhibitors. Since religation step requires nucleophilic attack of a free 5′-OH end to the phosphotyrosine bond, it is necessary that both should be in close proximity. Any factor that can cause misalignment between the phosphotyrosine and 5′-hydroxyl end is referred to as Top1 inhibitor, will stabilize the cleavage complex and prevent religation. Without religation, initially reversible single stranded DNA break collides with RNA polymerase during transcription or with DNA polymerase during replication resulting in double stranded breaks and leads to cell death [11].

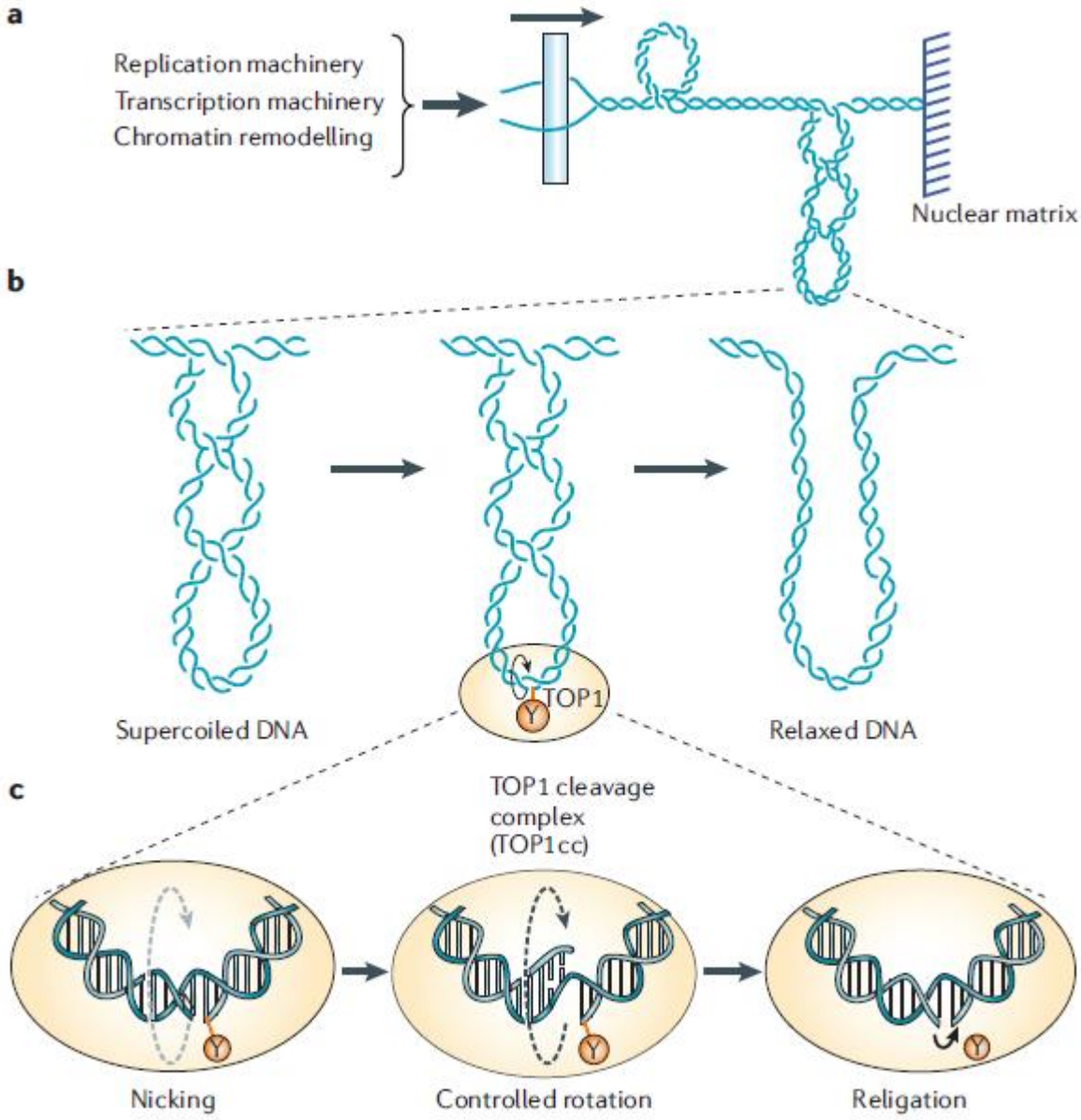

Figure 1.3. Mechanism for a) Supercoil formation b) DNA relaxation c) Top1 action [12].

1.2. Topoisomerase Inhibitor Camptothecin

Top1 has gained great attention after it was found that it is the sole target of the camptothecin class of antitumor drugs in the 80's [5,13]. One of the most renowned drug camptothecin (CPT) a noncompetitive inhibitor of Top1, is a plant alkaloid first isolated from the bark of *campthotheca acuminate*, an Asian tree known to exhibit antitumor activity well before it was found to target Top1 [14,15]. Cytotoxicity of CPT's are attributed to their inhibitory effect on the relaxation mechanism of the supercoils formed during DNA replication and their induction of double stranded breaks. CPT inhibits the religation step of

the Top1 catalyzed relaxation mechanism, resulting in accumulation of covalent reaction intermediate of Top1-DNA-CPT complex, referred to as the cleavage complex (Top1cc) [5]. Top1cc is a reversible protein-DNA covalent complex and acknowledged as a cellular lesion. CPT non-covalently interacts with flanking base pairs of DNA and Top1 active site amino acid residues to increase the half-life of the cleavage complex by preventing the enzyme from leaving (religation step). While the CPT-DNA-Top1 complex is reversible and non-lethal, collision of the replication fork causes double stranded breaks in DNA that cannot be repaired by any enzyme, and causes lethality as shown in Figure 1.4 [16].

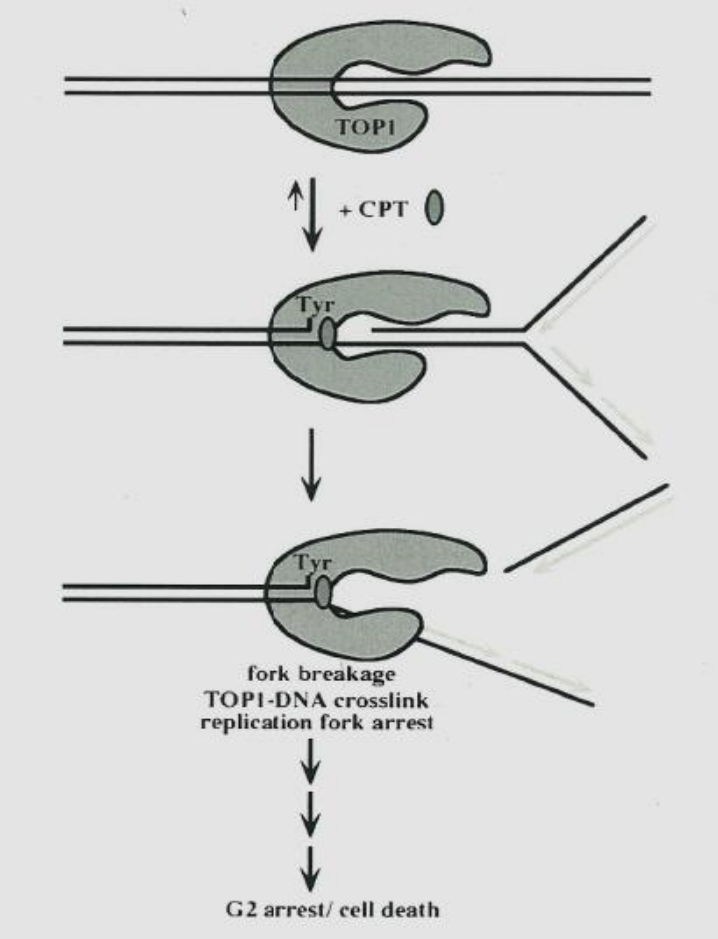

Figure 1.4. The working mechanism of cell death caused by Top1 targeting CPT anticancer drug [17].

There are several unique characteristics of CPT: (1) The natural 20*S* isomer of CPT alone shows inhibitory activity but not the synthetic 20*R* isomer. (2) Under physical conditions CPT neither binds to Top1 or DNA individually but rather binds to the cleavage

complex [18]. Selective inhibition of Top1-DNA complex by CPTs has been proven by deletion of Top1 gene from modified yeast cells resulting in CPT resistance [19]. Restoration of Top1 on plasmid however induced CPT sensitivity. Consecutively, overexpression of Top1 resulted in elevated levels of CPT toxicity and decreased levels of Top1 resulted in CPT resistance [20-22]. However, it has been extremely difficult to study the mechanism of camptothecin activity because the drug acts as an uncompetitive inhibitor and binds only to the transient enzyme substrate complex.

1.3. Camptothecin Analogue Topotecan

Today, many Top1-targeted anticancer drugs currently in clinical investigation are based on the CPT structure. Water soluble analogue of CPT, Topotecan (Hycamtin, GlaxoSmithKline) and Irinotecan (Camptosar, Pfizer) showing significant activity against solid tumors, have been approved by US Food and Drug Administration for the treatment of ovarian and small-cell lung cancers, colorectal cancers, respectively [23-25]. Hence, understanding their inhibition mechanism is crucial for the development of novel anticancer drugs. For this purpose, important sites for the drug binding on human Top1 enzymes were investigated by Top1 mutations [22]. There are several experimental studies which attempt to clarify the mechanism of CPT derivatives such as Topotecan. While one of these studies has shown that DNA sequence is not significant in the uncoiling rate and ternary complex stabilization [26], another one revealed the importance of the sequence selectivity in the camptothecin induced cleavage by human Top1 [27].

TPT or Topotecan (9-[(dimethylamino)methyl]-10-hydroxy-camptothecin), when compared to other members of the camptothecin family, has higher solubility and stability and lower toxicity which has enabled its successful use in treatment of ovarian and small cell lung cancers [28-30]. At physiological pH=7.4 TPT and other camptothecin derivatives are in equilibrium with their closed lactone and the E ring hydrolyzed open carboxylate forms (Figure 1.5) [31]. This pH dependent equilibrium shifts towards the lactone form under high acidic conditions (pH<4), and to carboxylate form under high basic conditions (pH>10) [32]. A kinetic model describing the equilibrium between open and closed forms of TPT concluded the equilibrium constant to be $1.98 \pm 0.07 \times 10^{-3}$ [33]. Moreover, it has been proven by NMR [34] and HPLC [35] studies that at pH 6.28 a 50:50 mixture of the two

forms of TPT is present. The carboxylate, open-ring form of Topotecan, predominates at physiological conditions. Carboxylate form of TPT lacks Top1 inhibiting activity and effectively binds to blood proteins [36,37]. This binding affinity of carboxylate form shifts the equilibrium to the right, therefore reduces the presence of active lactone form. Additionally carboxylate form has less than 10% the potency of the lactone form as a Top1 inhibitor [38], attributed to its low affinity for the active site of the cleavage complex and reduced membrane permeability [5,13]. The lactone form of TPT, the biologically active form, shows higher cytotoxicity but its mechanism of inhibition is poorly understood. The binding mode of active TPT was investigated with HPLC and NMR studies indicating that TPT binds to cleavage complex through intercalation [34]. It has been suggested that the double-stranded DNA stabilizes the active lactone form and promotes the conversion of the carboxylate form to the lactone form [39] and only the lactone form binds to the double- and single-stranded DNA in the absence of Top1 [34]. The crystal structure of the ternary complex (human Top1-DNA-TPT) was obtained in 2002 by Staker [16]. In the crystal structure the intercalation of TPT into the nicked region of the covalently bound DNA and Top1 complex is clearly observed. The crystallographic data also reveals the presence of carboxylate form of TPT, also regarded as the inactive form, in the intercalation pocket forming water-bridge hydrogen bonds with key amino acids [40]. While the crystal structure explains why the drug binds only to the enzyme – substrate complex by presenting specific hydrogen bond contacts with both the DNA and the enzyme, it provides no further explanation on the contribution of each amino acid residue or DNA to the inhibition process.

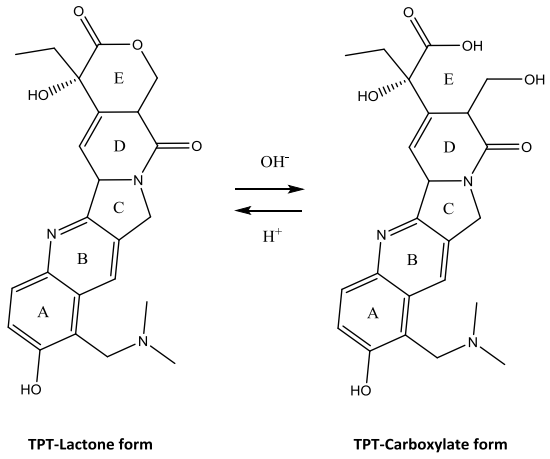

Figure 1.5. pH dependent hydrolysis of E-ring: equilibrium between TPT-lactone and TPT-carboxylate form (K= 1.98×10^{-3}).

The most significant understanding of the inhibitory mechanism was revealed in a Nature paper in 2007 [41]. In the study, Koster *et al*. carried out single molecule experiments to investigate the dynamics of the relaxation mechanism in the presence of TPT. They found that the drug molecule significantly slows down the DNA relaxation. The Topotecan-mediated uncoiling of positive DNA supercoils is reported to be around 20 times slower than that of wild type relaxation.

1.4. Intermolecular Interactions with TPT

Intermolecular interactions play a crucial role in a variety of biological processes, such as immune responses, enzymatic reactions, cell signaling, storage of genetic information and drug inhibition mechanisms. As in the case of inhibition of an enzyme by a drug, it is well known that the position and orientation of the interacting protein and the drug can drastically affect the strength of the interaction. Modern X-ray crystallography techniques can provide detailed three dimensional electron density maps and give a clue on non-covalent interactions. However, simply summarizing these interactions are inadequate for a mechanistic understanding of the inhibition. It is necessary to perform high level quantum mechanical calculations to quantify the strength of each intermolecular interaction and provide an insight into the inhibitory mechanism.

Computational studies on enzyme-inhibitor interactions have gained momentum in the last decade with the advances in computation algorithms and affordable computing times. Understanding enzyme-inhibitor intermolecular interactions has always centered around three non-covalent interactions namely: hydrogen bonding, electrostatic and hydrophobic interactions. More recently it become evident that π-π stacking plays a significant role as well. In this work intermolecular interactions between ligand (TPT) and enzyme (Top1) have been analyzed on the basis of a comprehensive conceptual framework that takes into account all of the mentioned non-covalent interactions.

1.5. Literature Study on Essential Interaction Site Residues

Lys532 and Arg364 are well-known residues in Top1 for their key role in the supercoil relaxation mechanism [42]. In recent molecular dynamics (MD) studies, the importance of

these residues is emphasized [43] and the dynamic properties of human Top1 are investigated [43-45]. NMR studies have also been performed to explain the binding mode of CPT to DNA [34,39,47,48]. Also, a combined experimental (UV-Vis) and computational strategy is used to analyze the electronic and structural properties of TPT in water at different pH values [49].

Top1 mutations were investigated in order to understand the importance of specific residues of Top1 in the relaxation mechanism of DNA. In principle, mutants that lead to drug resistance might identify the sites in Top1 that involve in a drug binding or some other enzymatic step that is essential for inhibition mechanism. Drug binding residues such as Asn722 and Thr718 in C-terminal domain mutations were investigated [50]. Asn722 is immediately in sequence to the catalytic Tyr723 and has been extensively examined because of its critical position. It has been concluded that while Asn722-Ser mutation causes CPT-resistance, it shows little impact on the catalytic activity of Top1. Meaning, while it is in close proximity to the catalytic Tyr723 residue, it has no contribution to DNA binding, strand cleavage or religation unlike Tyr723. This observation leads to the fact that Asn722 is a drug binding residue. Thr718-Ala mutation directly affected the relaxation rate even though the crystal structure has shown no direct or indirect contact between the drug and the residue.

In other studies mutations of Arg364 and Asp533 residues in core domain [51,52] has been discovered to result in TPT resistance. In the crystallography structure Asp533 is shown to form two contacts: one with TPT and the other with guanadino group of Arg364. It is emphasized that elimination of these residues would be expected to negatively impact the drug binding. Despite numerous experimental and molecular dynamics studies published, there is a very limited number of quantum chemical studies on this subject. One high level quantum chemical study using the MP2 method indicates that the binding orientations of non-camptothecin Top1 inhibitors such as indenoisoquinolines are primarily governed by π-π stacking [53]. This interaction is only observed between DNA and the drug so the study concludes that DNA has stronger interaction with the drug compared to the protein and better stabilizes the ternary complex. Molecular dynamics simulations involving mutation of Top1 and calculation of interaction energies of the wild type (not mutated) enzyme were conducted [54]. Three amino acid residue interaction energies with TPT are presented in this work: Lys425, Asp533 and Arg364 to be -6.52±2.26, -10.52±5.24 and -6.74±1.64 kcal/mol

respectively. While this work provides no further insight on the interaction of other residues in the active site, it provides us with a relative comparison for three residue interaction energies. This work also states that the strongest interaction is observed for Asp533, and the interactions of Lys425 and Arg364 with TPT are very close to each other.

2. AIM OF THE STUDY

In this study, quantum chemical calculations were carried out following the atomistic molecular dynamic simulations performed by Levent Sarı from Fatih University. The aim of this study is to gain a better understanding on the interactions in the ternary complex DNA-Top1-TPT. The focus of the study is to elaborate individual non-covalent interactions between i) TPT and DNA, ii) TPT and protein. The relative energetic strengths of TPT-DNA and TPT-protein interactions will provide us with the estimates of crucial interactions in the stabilization of the ternary complex justifying the reason why TPT can be used as an anti-cancer drug.

3. METHODOLOGY

In this chapter the aim is to define some theoretical approaches used in this study namely: Density Functional Theory (DFT), basis sets, Polarizable Continuum Model (PCM), semi-empirical methods. Semi-empirical calculations were performed using MOPAC2012 and quantum chemical calculations were performed by Gaussian ’09.

3.1. Density Functional Theory

Density Functional Theory (DFT) is a quantum mechanical approach that is based on the theorem of Hohenberg and Kohn. This theorem states that with known electron density one can describe the ground state properties of a molecule. The major goal of DFT is to solve the non-relativistic time-independent Schrödinger equation:

$$H\Psi = E\Psi \tag{3.1}$$

where H is the Hamiltonian operator the solution of Schrödinger equation gives system energy E as an eigenvalue described by the wave function Ψ. Schrödinger equation has many acceptable eigen functions Ψ, each one yields a different eigenvalue, meaning that it has infinite set of solutions. Therefore for each Ψ_i wavefunction there is an eigenvalue E_i:

$$H\Psi_i = E\Psi_i(X), n = 1, 2, 3 \ldots \tag{3.2}$$

Equation 3.2 can be easily solved for small systems. However, infinite number of solutions causes finding the exact solution for many electron systems. Since the Hamiltonian for the electron-electron interaction term is too complex. Finding the solution with approximations is one way in which the wave function of the whole system should be written as the product of many electron systems.

Eigen functions can be broken down into one electron like systems:

$$\Psi_{HP} = \Psi_1 \Psi_2 \dots \Psi_N \tag{3.3}$$

this is the Hartree Product and it treats each electron system independently.

Hamiltonian operator can be broken down into kinetic and potential terms:

$$H = T + V \tag{3.4}$$

The Hamiltonian depends on the positions and atomic numbers of the nuclei and all the electrons and it can be broken down to several components:

$$H = -\sum_i \frac{\hbar}{2m_e}\nabla_i^2 - \sum_i \frac{\hbar}{2m_k}\nabla_k^2 - \sum_i \sum_k \frac{e^2 Z_k}{r_{ik}} + \sum_{i<j} \frac{e^2}{r_{ij}} + \sum_{k<l} \frac{e^2 Z_k Z_l}{r_{kl}} \tag{3.5}$$

where the first two term is the kinetic energy of electron and nuclei respectively, the third term is the electron-nuclei interaction, the fourth and fifth term is the exchange-correlation for electron–electron repulsion and Coulomb repulsion respectively. Dependence of Hamiltonian on the total number of electrons can be obtained by integrating the electron density ρ over all space:

$$N = \int \rho(\mathrm{r}) d\mathrm{r} \tag{3.6}$$

Electron density ρ(r) determines the external potential due to nuclei V(r):

$$\rho(\mathrm{r}) = N \int \dots \int |\Psi(r_1, r_2, \dots r_n)|^2 dr_1, dr_2, \dots dr_n \tag{3.7}$$

where r_i represents the coordinates of the electrons. Any electron density evaluated with DFT except the real one will present higher energy compared to ground state.

Ground state electronic energy can be presented as a function of electron density:

$$E[\rho(\mathrm{r})] = \int V(r)\rho(\mathrm{r})d\mathrm{r} + T[\rho] + V[\rho] \tag{3.8}$$

Where the first term is for the interaction of electrons with external potential, $T[\rho(\mathrm{r})]$ term is kinetic energy of electrons and $V[\rho(\mathrm{r})]$ is the electron-electron interaction energy. Electronic energy can be expressed as:

$$E[\rho(\mathrm{r})] = \int V(r)\rho(\mathrm{r})d\mathrm{r} + T_S[\rho] + J[\rho] + E_{XC}[\rho] \tag{3.9}$$

where $T_S[\rho]$ is the kinetic energy of non-interacting electrons, $J[\rho]$ is the coulomb and $E_{XC}[\rho]$ is the exchange-correlation and correction for real kinetic energy of the system. Although exchange-correlation $E_{XC}[\rho]$ is the kinetic energy difference between interacting and non-interacting electron systems it is expressed as the sum of quantum mechanical exchange $E_X[\rho]$, correlation $E_C[\rho]$ and correction term for classical self-interaction energy. The Coulomb energy term is the repulsion arising from the electron repulsion.

The exact value of exchange correlation functional is unknown. There are several approximations used to calculate it and the first one is the Local Density Approximation (LDA). LDA divides non-homogenous system and considers the electron density uniformly distributed. Hence this method is not applicable to highly delocalized electron density systems. $E_{XC}[\rho]$ can be expressed with this approximation as:

$$E_{XC}[\rho(\mathrm{r})] = \int \rho(\mathrm{r})\varepsilon_{XC}\big(\rho(\mathrm{r})\big)dr \tag{3.10}$$

$\varepsilon_{XC}\big(\rho(\mathrm{r})\big)$ can be differentiated to give the exchange-correlation functional $V_{XC}[\rho(\mathrm{r})]$:

$$V_{XC}[\rho(\mathrm{r})] = \rho(\mathrm{r})\frac{d\varepsilon_{XC}\big(\rho(\mathrm{r})\big)}{d\rho(\mathrm{r})} + \varepsilon_{XC}\big(\rho(\mathrm{r})\big) \tag{3.11}$$

Kohn Sham Hamiltonian expressed as h_{KS} is :

$$h_{KS}\phi_i = \varepsilon_i\phi_i \tag{3.12}$$

One of the functional used for this purpose, M06-2X is a Minnesota 06 generation global hybrid functional based on meta-GGA approximations. It takes into account double amount of nonlocal exchange (2X) and employs 54% Hartree-Fock exchange. It is parametrized to take into account long range and non-covalent interactions [55].

$$E_{XC}^{hyb} = \frac{X}{100}E_X^{HF} + \left(1 - \frac{X}{100}\right) E_X^{DFT} + E_C^{DFT} \tag{3.13}$$

where E_X^{HF} is the nonlocal Hartree–Fock (HF) exchange energy, X is the percentage of Hartree–Fock exchange in the hybrid functional, E_X^{DFT} is the local DFT exchange energy, and E_C^{DFT} is the local DFT correlation energy.

Another functional is a long-range corrected (LC) hybrid density functional ωB97XD it employs 100% Hartree-Fock exchange for long-range interactions between electrons and 22% for short-range. The total energy is computed by:

$$E_{DFT-D} = E_{KS-DFT} + E_{disp} \tag{3.14}$$

as the sum of a KS-DFT part, using the ωB97X functional, and an empirical atomic-pairwise dispersion correction. The exchange is written as:

$$E_{XC} = c_X E_X^{HF} + E_{XC}^{DFA} \tag{3.15}$$

where c_X is a small fractional number, typically ranging from 0.2 to 0.25 for thermochemistry, and from 0.4 to 0.6 for kinetics.

M06-2X and ωB97XD functionals were used since they were reported to be suitable for the prediction of energies for structures with non-covalent interactions [55].

3.2. Solvation Model

Biological processes like drug-enzyme interactions take place in solvent containing medium in living organisms. It is necessary to include solute-solvent interactions in order to evaluate the intermolecular interaction in biological system appropriately. Computational methods can be separated into two based on their treatment of solvation: explicit and implicit solvation model. In continuum solvation which is an implicit solvation method, the solvent is treated as a homogenous medium having a single dielectric constant (Ɛ). Dielectric constant is set to be equal to bulk value of solvent. Solute is embedded into a cavity surrounded by the solvent medium.

$$\Delta G_{solvation} = \Delta G_{cavity} + \Delta G_{dispersion} + \Delta G_{electrostatic} + \Delta G_{repulsion} \qquad (3.16)$$

where the first term represents the energy cost of placing the solute into the solvent cavity. The second term is dispersion interaction between solvent and solute which adds stabilization to solvation free energy. The third term represents the interaction energy between solute and solvent. The final term is the exchange interactions of solute-solvent not included in the cavitation energy.

3.3. Semi-empirical Methods

Semi-empirical approach was developed to overcome the computational cost of integral calculations. This method exploits the fact that chemical properties can be described with valence electrons and draws the core electrons into the nuclear center. The most demanding step of HF calculations are the two electron integrals appearing in Fock matrix:

$$F_{\mu\nu} = \left\langle \mu \left| -\frac{1}{2}\nabla^2 \right| \nu \right\rangle - \sum_{k}^{nuclei} Z_k \left\langle \mu \left| \frac{1}{r_k}\nabla^2 \right| \nu \right\rangle + \sum_{\lambda\sigma} P_{\lambda\sigma} \left[(\mu\nu|\lambda\sigma) - \frac{1}{2}(\mu\lambda|\nu\sigma) \right] \qquad (3.17)$$

not only solving the integrals are tedious but also there are many of them (N^4 where N is the number of basis functions). One way to save computational time is to accurately estimate their value beforehand. Especially for integrals in large molecules, one can avoid calculating very large integrals by assuming them to be zero.

The earliest semi-empirical method was MNDO, it was advantageous because it was

parametrized to reproduce molecular properties instead of atomic ones [56]. At first, it was widely used because it increased accuracy. However, in time various limitations were found. Among the most important of which was the lack of hydrogen bonding contribution. As hydrogen bonding is essential in biochemical systems this method's particular defect was precluding its use in biological system.

The lack of hydrogen bonding contribution in MNDO semi-empirical methods have been improved by the AM1 method, which over simplified the complicated hydrogen bonding phenomenon, to core-core interactions [57]. In the coming years several improvements were made to the semi-empirical method and the parametrization. The resulting method was PM3 which was developed by Stewart [58]. He predicted that AM1 had been non-optimal because optimization of parameters was done in stepwise fashion, which would give rise to accumulating errors. That is why, in PM3 method simultaneous optimization of the parameters for main elements was adopted. Various changes to MNDO approximations were introduced such as addition of *d*-orbitals to the main group elements and addition of diatomic parameters.

The PM6 method is the most recent and accurate addition to the MNDO family of semi-empirical approximations [59]. Like PM3 method it was developed by Stewart and has been parametrized guided by the errors found in earlier methods. It was built on the PM3 method but differing in: core-core interactions, addition of transition metals, unpolarizable cores. Low energy interactions such as intermolecular interactions can be better expressed with this method. This is why it is the best semi-empirical method that can be used in biological systems which includes a large variety of non-covalent interactions. Despite the improvement in hydrogen bonding corrections, there were significant errors in zwitterions. The main advantage of the PM6 method is in particular it was parametrized to reproduce ΔH_f taking into consideration the B3LYP functional [60] in DFT. It is stated that PM6 shows comparable performance in equilibrium systems. However, when non-equilibrium systems are considered, especially for transition state geometries, PM6 is inferior compared to B3LYP.

PM6-DH+ method, also known to be a third-generation hydrogen-bonding correction procedure, is used to correct the errors that are observed in the PM6 method. This method

was chosen because it was parametrized for the non-covalent interaction energies obtained from advanced quantum mechanical calculations (DFT). Compared to previous semi-empirical approaches, empirical corrections for dispersion and hydrogen-bonding interactions were included to gain a better understanding on interaction energies of biological systems [61]. The advantage of using third-generation correction instead of first or second is because it does not make hydrogen bond acceptor/donor assumptions unlike the first two generation corrections. Instead, it regards the hydrogen bond as being charge independent between two atoms that can be viewed as an acceptor or a donor.

$$E_{H-bond} = \frac{C_{AB}}{r_{AB}^2} f_{geom} \times f_{damp} \tag{3.18}$$

where C_{AB} is the corresponding hydrogen-bonding correction parameter for A and B hydrogen donor/acceptor atoms. The damping function f_{damp} is activated for larger molecules to accurately identify the hydrogen bonding distance. Geometry function f_{geom} is used to define the torsion angles.

3.4. Computational Details

Semi-empirical calculations with MOPAC 2012 [62] were used for geometry optimizations of the selected active site obtained from 3 ns long molecular dynamics simulation. PM6-DH+ method was used to correct the errors that are observed in PM6 method. This method was chosen because it was parametrized for the interaction energies obtained from advanced quantum mechanical calculations (DFT). Compared to previous semi-empirical approaches empirical corrections for dispersion and hydrogen-bonding interactions were included to gain a better understanding on interaction energies of biological systems [61]. One of the previous semi-empirical methods, PM6 was used to observe the difference between PM6-DH+ method. Indeed, both in vacuum and water optimizations with PM6 method protonation of TPT has occurred. This geometry is undesired because it disrupts the aromaticity of the A ring in TPT.

Optimizations with MOPAC were carried out in several steps. Keywords MOZYME and MMOK were used to include Localized Molecular orbital method and molecular

mechanics correction to NHCO bonds. EPS keyword was chosen to activate COSMO [63] (Conductor-like Screening Model) method to approximate the effect of surrounding solvent. In optimization calculations EPS is 78.4 and 4, to set the dielectric constant (Ɛ) for water and protein respectively.

Optimization of the whole complex with advanced quantum mechanical calculations (ωB97XD/6-31G(d)) in gas phase was carried out with Gaussian09.

Following optimization with both Gaussian and MOPAC, single point calculations were carried out to accurately quantify the interactions energies. The Gaussian09 program package [64] was used for the single-point calculations with M06-2X/6-31+G(d,p) and ωB97XD/6-31+G(d,p) methods, which are suitable for the prediction of energies for structures with non-covalent interactions [55].

4. RESULTS AND DISCUSSION

4.1. Optimization Results

Selected active site for the quantum chemical calculations was constructed from residues and DNA layers within 8 Å radius from TPT. The amino acids considered were chosen not only because of their proximity to the active site but also because they have been reported to be important for the stabilization of the cleavage site. The employed model includes 4 layers of DNA base pairs, 8 amino acid residues and the drug TPT seen in Figure 4.1.a. Methyl groups were introduced to the ends of the outer layer DNA and to the ends of amino acid residues. These methyl groups were frozen during all geometry optimizations.

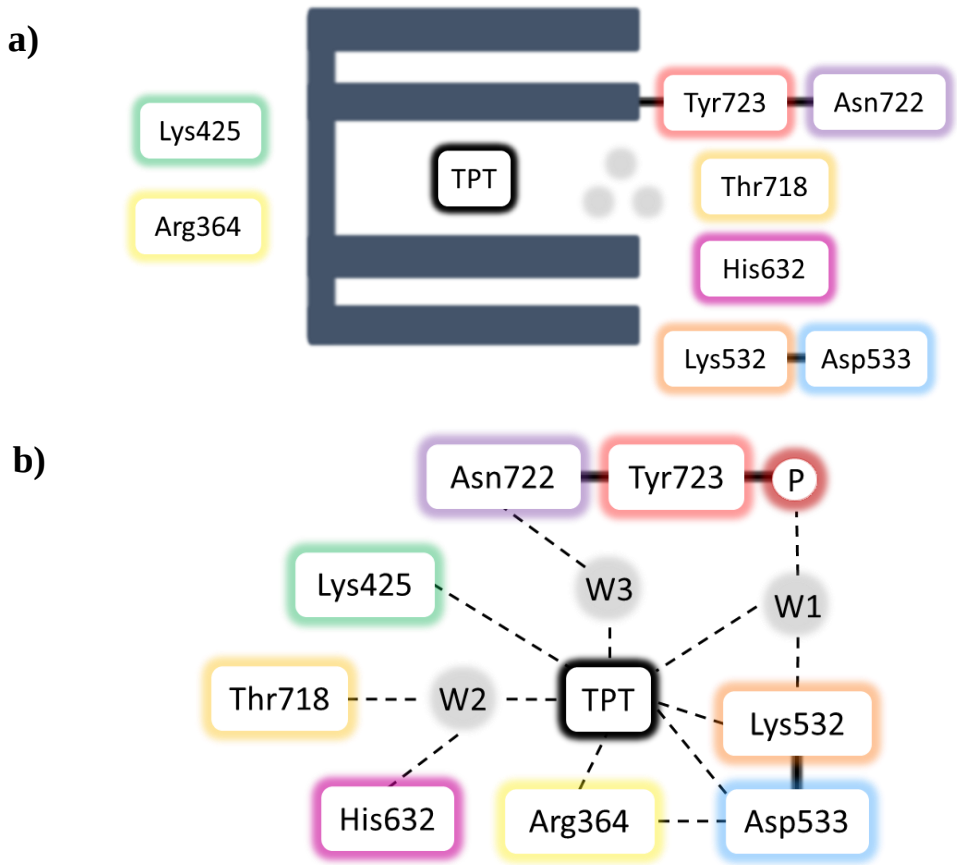

Figure 4.1. Simplification of selected sites for quantum mechanical calculations (after 3ns MD). a) Representation of active site. b) TPT-Residue interaction map (the DNA layers are not shown for clarity).

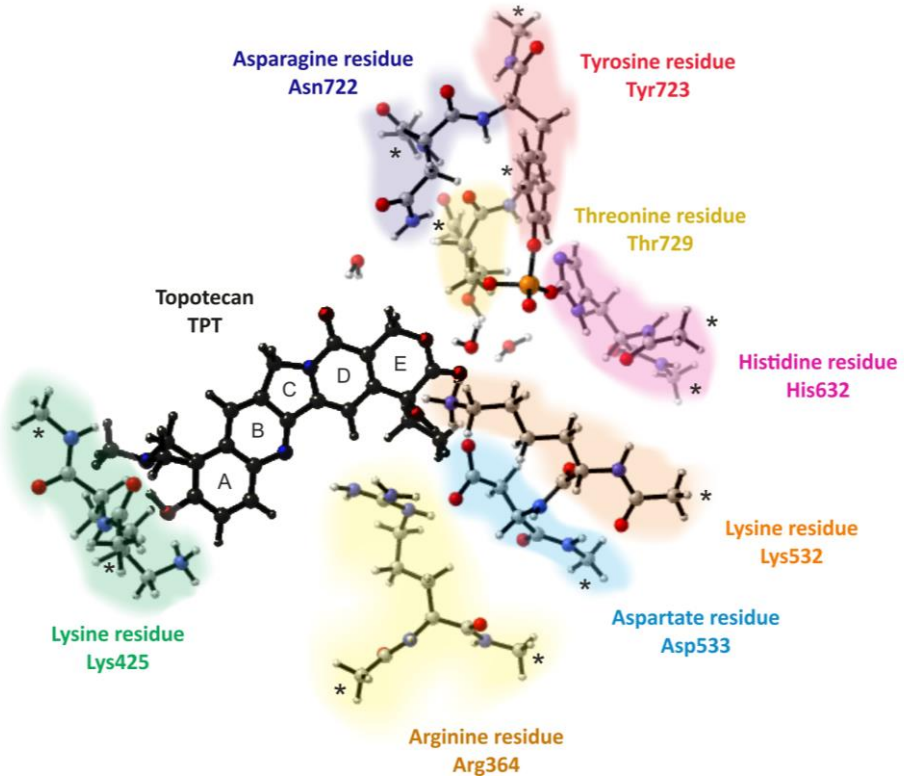

Figure 4.2. Selected sites for quantum mechanical calculations. (The 4 DNA layers are not shown for clarity).

Optimization of the active site was carried out in three steps:

(i) Hydrogen optimization with heavy atoms (any atom other than hydrogen) frozen.

(ii) Optimization of the system with: frozen DNA base pairs, residue backbones and residue methyl ends (indicated in Figure 4.2 with asterisks), outermost layers of DNA represented in Figure 4.1 a) as blue boxes.

(iii) Complete system optimization with only amino acid methyl ends and outermost layers of DNA frozen.

Optimized structures with PM6-DH+ and ωB97XD method were compared to see if the semi-empirical method was able to reach the accuracy of the expensive DFT method. Between the optimization methods it is observed that the structure of TPT differs slightly in A and E rings. The resulting DNA structures are exactly the same for outermost layers as expected since they were frozen in optimization. The intact backbone of DNA is Figure 4.3.a changed between two optimization methods. For residues the largest difference is observed for His632, W1 and W2. His632 acts as a hydrogen-acceptor with PM6-DH+ and as a

hydrogen-donor with ωB97XD optimization method. It can be said that in PM6-DH+ method electrostatic interactions are more important compared to ωB97XD. Since charged residues are in close proximity: Arg364-Asp533-Lys532 drawn together.

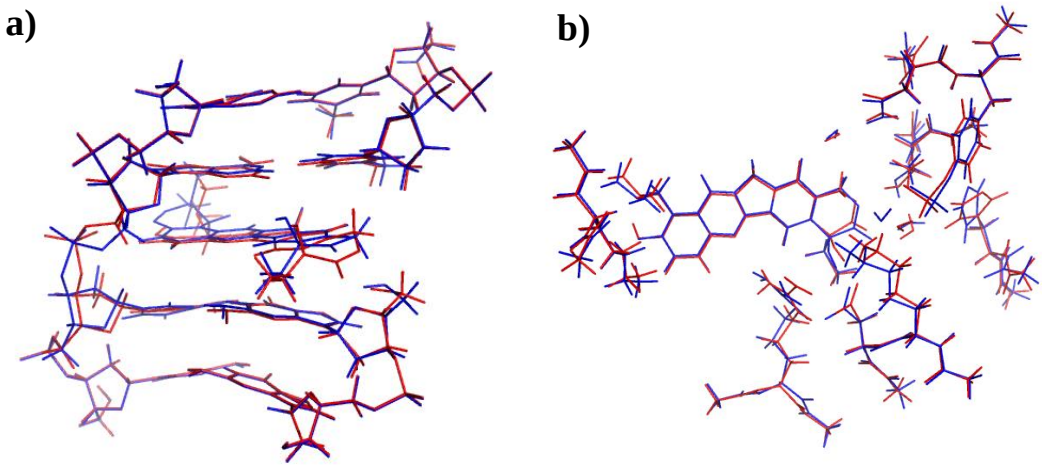

Figure 4.3. Comparison of PM6-DH+ protein phase in blue and ωB97XD in red optimized structures. a) DNA-TPT and b) TPT-Residue.

Table 4.1. Interaction distances (Å) in selected active site after MD, optimization with PM6-DH+ (Ɛ=78.4), PM6-DH+ (Ɛ=4) and ωB97XD/6-31G(d) methods.

	MD (3ns)	PM6-DH+ (Ɛ=4)	ωB97XD
PTyr723-W1	1.87	1.74	1.76
Asn722-W3	2.35	1.83	1.86
Arg364-TPT	3.35	2.51	2.62
Thr718-W2	1.86	1.66	1.78
Lys425-TPT	1.69	1.74	1.90
His632-W2	2.85	2.50	1.88
Asp533-TPT	2.02	1.71	1.75
Lys532-TPT	2.76	2.44	2.55
Lys532-W1	1.73	1.71	1.70
W1-TPT	1.97	1.86	3.08
W2-TPT	1.78	1.76	2.10
W3-TPT	1.72	1.89	1.88

Interaction distances (Å) presented in Table 4.1 compares the initial (3ns MD), after optimization with PM6-DH+ in both water and protein and finally gas phase optimization with ωB97XD methods. Contraction in the distances after optimization with all methods are seen for PTyr723-W1, Asn722-W3, Arg364-TPT, Thr718-W2, His632-W2, Asp533-TPT,

Lys532-TPT compared with MD distances. Other distances with different optimization methods are comparable except for W1-TPT, W2-TPT and His632-W2 distances. It can be observed by looking at the interaction distances alone W1-TPT and consecutively water-bridging residues with W1 (PTyr723 and Lys532) are expected to show a huge difference in interaction energies with ωB97XD method.

4.2. Separation of Covalently Bound Residues

After optimizations the main aim is to accurately quantify the contribution of each amino acid residue to the overall interaction with TPT. For this purpose, covalently bound residues were separated. Covalently bound residues are Tyr723-DNA, Tyr723-Asn722 and Lys532-Asp533.

Catalytic Tyr723 residue was separated from the DNA layer by breaking the phosphate sugar bond (Figure 4.4). Ruptures in covalent bond are shown in red line. New tyrosine fragment is denoted as PTyr723 because it includes phosphate. Phosphate is a part of DNA and breaking the bond so that it stays with tyrosine residue fragment, can be misleading. But we know that most of the interaction of DNA with TPT is caused by π-π stacking interactions[53]. Hence, this fragmentation method is not expected to decrease the interaction energy of DNA considerably. Methyl cap was introduced to new PTyr723 fragment. For the fragmented DNA a hydrogen was introduced where the covalent bond was broken.

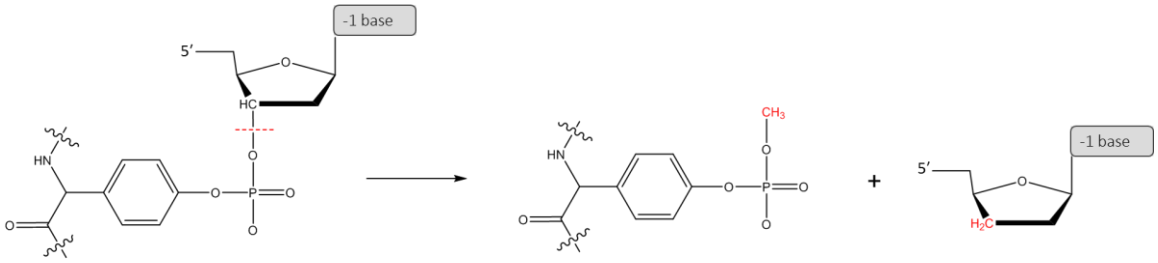

DNA-Tyr723 PTyr723 DNA

Figure 4.4. Cleavage of catalytic Tyr723 residue from DNA.

For amino acid residues covalently bound to each other (Lys532-Asp533 and PTyr723-Asn722) ruptures were introduced in between the peptide bond (Figure 4.5). Resulting two fragments were capped to preserve the peptide bond and an additional methyl groups were added.

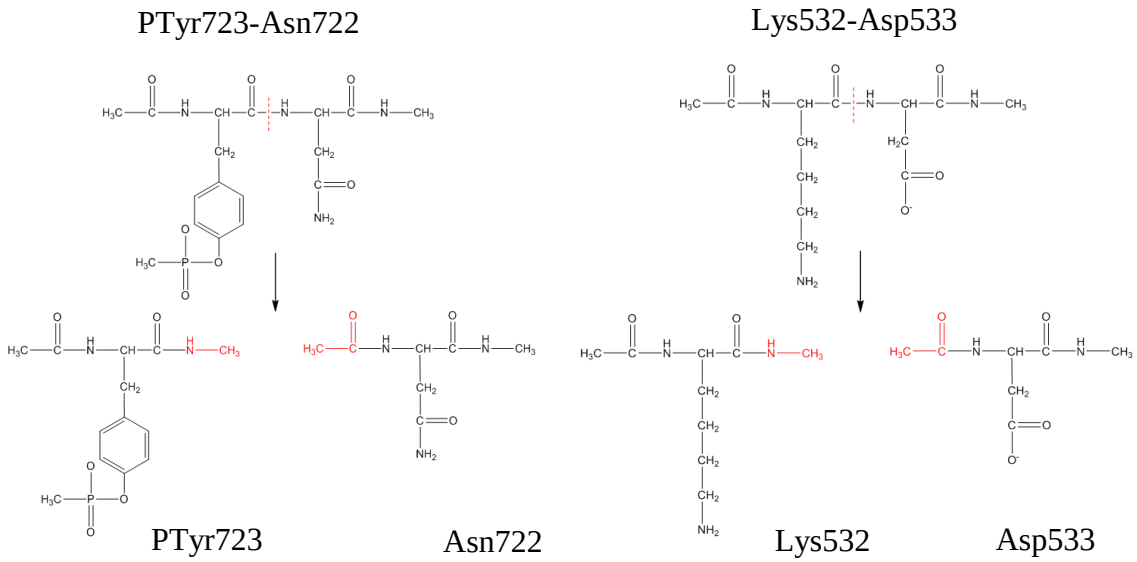

Figure 4.5. Cleavage of two covalently bonded residues, PTyr723-Asn722 and Lys532-Asp533.

4.3. Interaction Energy Calculations for Residues

Interactions of waters and residues are presented in Figure 4.6 after PM6-DH+ and ωB97XD/6-31G(d) optimization. Only the interacting and neighboring ring was presented in TPT structure with the corresponding residue and if present, water molecule.

The detailed interaction characteristics of each residue can be discussed by looking at Figure 4.6. The rough comparison between two optimization methods was discussed in Figure 4.3 and it is stated that the His632 residue changes from being an hydrogen acceptor to hydrogen donor residue. Another residue PTyr723, while no change in the interaction manner is observed its hydrogen bonding atom differs between two methods.

PM6-DH+ (Ɛ =4)	ωB97XD/6-31G(d)
PTyr723-TPT interaction	
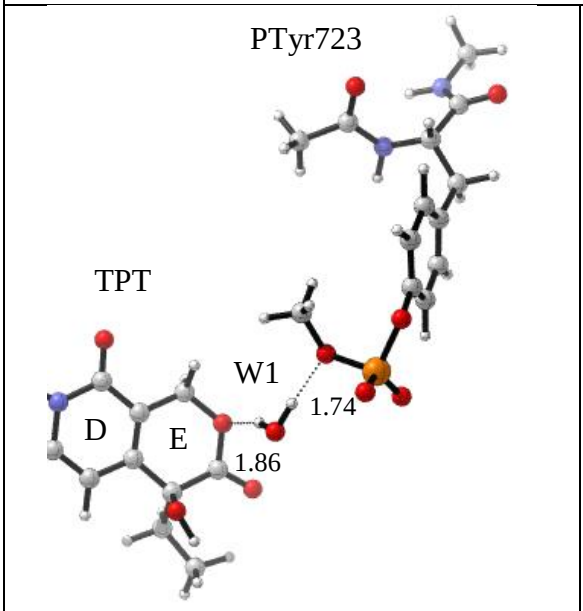	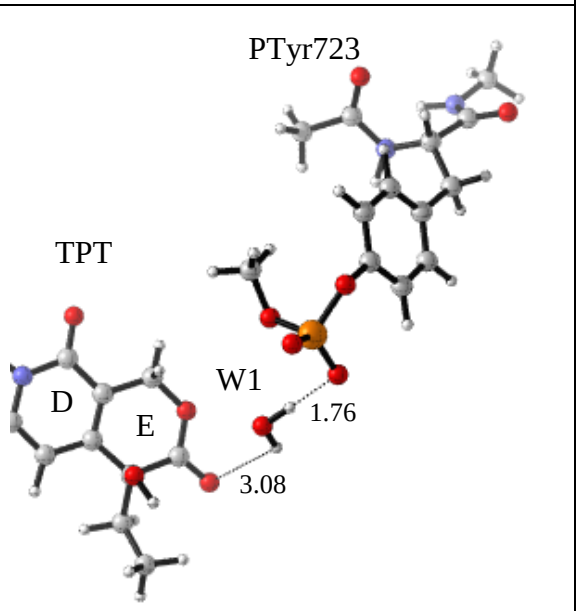
Asn722-TPT interaction	
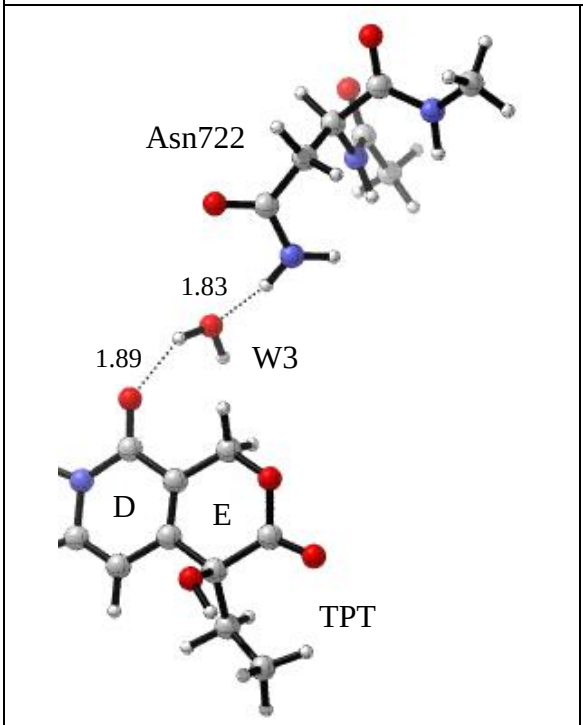	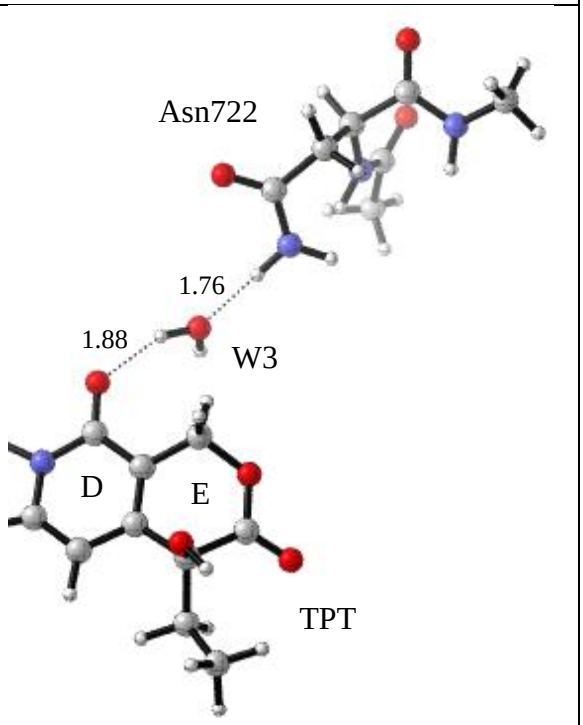

Figure 4.6. Comparison of the interacting PTyr723 and Asn722 residues and waters (PM6-DH+ optimization in first and ωB97XD in second column).

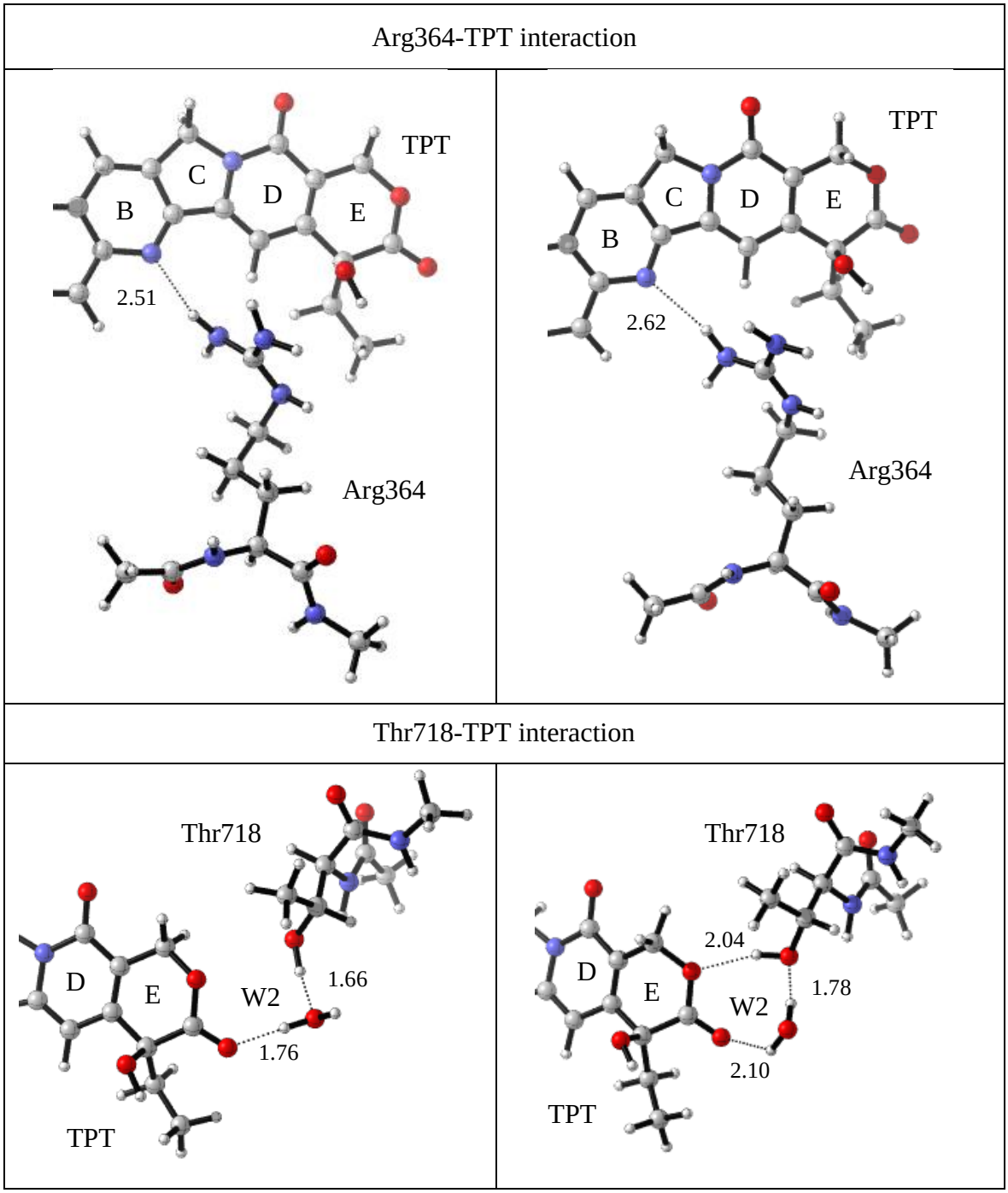

Figure 4.7. Comparison of the interacting Arg364 and Thr718 residues and waters (PM6-DH+ optimization in first and ωB97XD in second column).

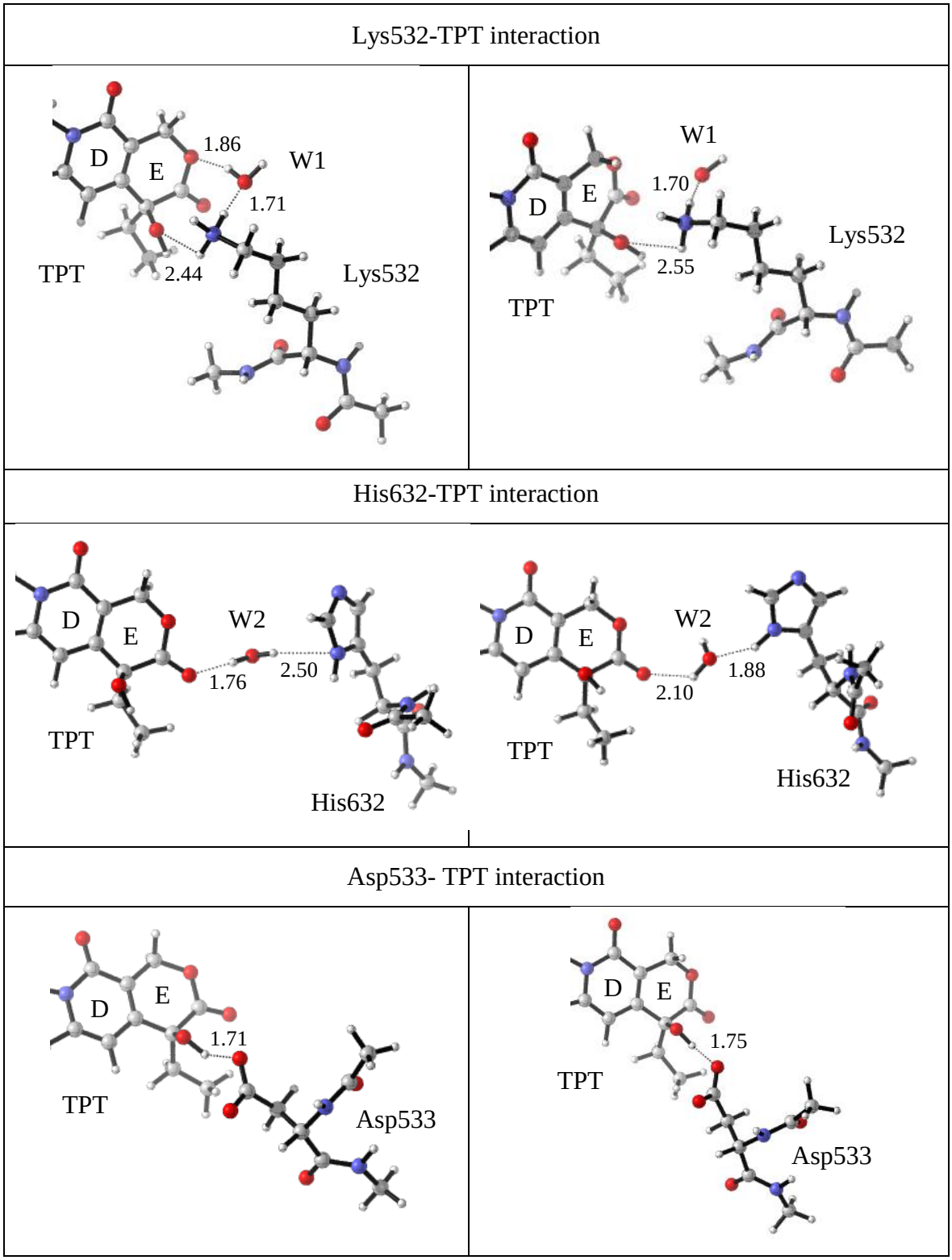

Figure 4.8. Comparison of the interacting Lys532, His632 and Asp533 residues and waters (PM6-DH+ optimization in first and ωB97XD in second column).

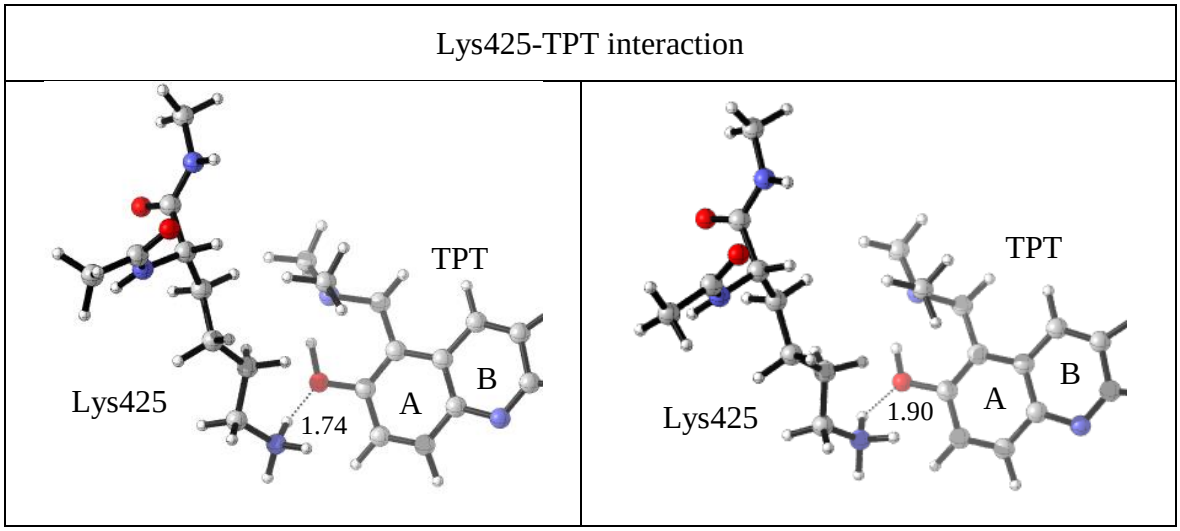

Figure 4.9. Comparison of the interacting Lys425 residues and waters (PM6-DH+ optimization in first and ωB97XD in second column).

The most notable change between two optimization methods is clearly observed in Thr718 residue. With PM6-DH+ method the interaction between TPT and Thr718 is only maintained by a water bridge. However, this changes with the ωB97XD optimization where Thr718 establishes a direct interaction with the TPT while the water bridge remains intact. This result can be the outcome of the long range correction of ωB97XD functional, which enables the accurate optimization of distant interactions. Another notable change is seen for Lys532 residue which interacts directly and through a water bridge with the TPT in PM6-DH+ method. Albeit the presence of a water bridge in addition to the direct interaction would result in a stronger interaction, ωB97XD disrupts the preexisting water bridge. This indicates while ωB97XD optimizations are advantageous for long range interaction, they can be unreliable for the calculation of short range interactions such as Lys532.

4.3.1. **TPT Residue Interactions Without Water Contributions**

The interaction energy (ΔE_{INT}) calculation, is carried out with the supramolecular method:

$$\Delta E_{INT} = E_{R-TPT} - E_{TPT} - E_R \tag{4.19}$$

where $E_{R\text{-}TPT}$ is the single point energy for the residue and TPT complex. E_{TPT} and E_R is the single point energy of TPT and residue separately. With this interaction energy calculation method, the contribution of the water to the interaction of residues are ignored. Residues interacting with TPT only by water bridges (PTyr723, Asn722, His632 and Thr718) are expected to have low interactions. On the other hand, residues interacting with TPT directly through a hydrogen bond (Lys425, Arg364, Asp533 and Lys532) are expected to have higher interaction energies. The three water molecules (W1, W2 and W3) were treated like residues and their interaction energy were calculated separately. Only the closed-lactone form of TPT was used due to the lack of open-carboxylate form molecular dynamics simulation.

Table 4.2. Interaction energies (kcal/mol) of residues and water molecules with M06-2X/6-31+G(d,p) and ωB97XD/6-31+G(d,p)//PM6-DH+ (Ɛ=4).

	M06-2X/6-31+G(d,p)[a]//PM6-DH+ (Ɛ=4)		
	[a] Ɛ=0	[a] Ɛ=78.4	[a] Ɛ=4
PTyr723	5.58	-0.12	1.67
Asn722	-0.76	-0.28	-0.45
Arg364	-13.17	-4.61	-6.30
Thr718	-3.68	-0.75	-1.58
Lys425	-20.74	-5.46	-8.87
His632	0.17	-0.03	0.04
Asp533	-12.32	-6.25	-7.05
Lys532	-15.48	-1.18	-4.53
W1	-3.06	-2.60	-2.69
W2	-4.85	-3.15	-3.62
W3	-4.26	-2.31	-2.81
	ωB97XD/6-31+G(d,p)[a]//PM6-DH+ (Ɛ=4)		
	[a] Ɛ=0	[a] Ɛ=78.4	[a] Ɛ=4
PTyr723	5.11	-0.59	2.15
Asn722	-1.16	-0.68	-0.77
Arg364	-15.22	-6.83	-7.84
Thr718	-4.52	-1.54	-2.59
Lys425	-23.48	-8.24	-11.6
His632	-0.10	-0.31	-0.19
Asp533	-12.53	-6.40	-5.94
Lys532	-16.67	-2.48	-4.89
W1	-2.79	-2.33	-2.26
W2	-4.93	-3.20	-3.85

W3	-3.98	-2.04	-2.64

[a] Single point calculations in gas phase (Ɛ=0), PCM correction in water (Ɛ=78.4), PCM correction in protein (Ɛ=4)

Interaction energies calculated with M06-2X/6-31+G(d,p)//PM6-DH+ (Ɛ=4) method in gas, water and protein phase are presented in Table 4.2. PTyr723 and His632 residues show unfavorable repulsive interactions in both gas and protein phase calculations. For calculations in water phase Tyr723 and His632 shows little change in the order of -0.12 and -0.03 kcal/mol respectively. The other residues and waters (W1, W2 and W3) show favorable interactions with TPT. The strongest and weakest interactions vary with phase difference. The strongest favorable interaction in protein and gas phase is seen for Lys425 residue while in water phase for Asp533 residue. This is expected since these residues have the smallest interaction distance. Interaction energies calculated with ωB97XD/6-31+G(d,p)//PM6-DH+ (Ɛ=4) method in gas, water and protein phase are presented in the second part of Table 4.2. Comparing the results with M06-2X single point calculations, we observe that now only PTyr723 gives repulsive positive interaction with higher magnitude. The strongest interaction is similarly seen again for Lys425 with higher magnitude. The second strongest interaction however changes from Asp533 to Arg365. This result is unexpected because considering the two residues, both have direct interactions with TPT and Asp533 (1.71 Å) has the smaller interaction distance compared to Arg356 (2.51 Å).

Table 4.3. Interaction energies (kcal/mol) of residues and water molecules with M06-2X/6-31+G(d,p) and ωB97XD/6-31+G(d,p)//ωB97XD/6-31G(d).

	M06-2X/6-31+G(d,p)[a]//ωB97XD/6-31G(d)		
	[a] Ɛ=0	[a] Ɛ=78.4	[a] Ɛ=4
PTyr723	1.88	-0.29	1.08
Asn722	-0.77	-0.30	-0.57
Arg364	-10.25	-4.00	-4.26
Thr718	-4.43	-3.39	-3.70
Lys425	-16.29	-3.99	-6.15
His632	-1.36	-0.05	-0.60
Asp533	-16.07	-7.45	-8.37
Lys532	-9.07	0.26	-0.29
W1	-2.82	-0.95	-1.44

W2	-5.20	-2.12	-3.28
W3	-7.54	-4.63	-5.58

Table 4.3. Interaction energies (kcal/mol) of residues and water molecules with M06-2X/6-31+G(d,p) and ωB97XD/6-31+G(d,p)//ωB97XD/6-31G(d) (cont.).

	ωB97XD/6-31+G(d,p)[a]//ωB97XD/6-31G(d)		
	[a] Ɛ=0	[a] Ɛ=78.4	[a] Ɛ=4
PTyr723	1.58	-0.55	0.81
Asn722	-1.29	-0.51	-0.78
Arg364	-12.54	-6.42	-6.64
Thr718	-4.73	-3.72	-4.02
Lys425	-18.34	-6.08	-8.20
His632	-1.53	-0.19	-0.75
Asp533	-16.21	-7.51	-8.46
Lys532	-9.85	-0.74	-1.19
W1	-2.66	-0.74	-1.26
W2	-4.90	-1.76	-2.95
W3	-7.56	-4.61	-5.57

[a] Single point calculations in gas phase (Ɛ=0), PCM correction in water (Ɛ=78.4), PCM correction in protein (Ɛ=4)

Interaction energies calculated with M06-2X/6-31+G(d,p)//ωB97XD/6-31G(d) method in gas, water and protein phase are presented in Table 4.3. The interaction results obtained from ωB97XD optimized structure differs from the PM6-DH+ optimized ones. The strongest interactions in protein phase are seen for Asp533 and then Lys425 residue. This result can be attributed to the change in the interaction distance of Lys425 to TPT with ωB97XD (1.90 Å) method compared to PM6-DH+ (1.74 Å) method. For ωB97XD optimized structures, an elongation in distance is observed for Lys425 by 0.16 to 0.22 Å compared to PM6-DH+. Hence the decrease in interaction energy is expected. While the distance of Asp533 differs only by 0.03 Å an insignificant change in the distance, renders the interaction of Asp533 strongest. Interaction energies calculated with ωB97XD/6-31+G(d,p)//ωB97XD/6-31G(d) method in gas, water and protein phase are presented in the second part of Table 4.3. As expected, with ωB97XD optimization the interaction energy of Thr718 is stronger (-4.02 kcal/mol) compared the PM6-DH+ optimization (-2.59 kcal/mol). This is the result of establishment of a direct hydrogen bond contact between TPT and Thr718 with ωB97XD. The strongest interaction is similar to first part of the Table 4.3 and it is with Asp533. However, this time the interaction difference between Lys425 and Asp533

is smaller than single point calculation done with M06-2X in protein phase. This result is desired because it is similar to the work done by Pan *et al* in which it is stated that the two charged residues interaction energies are similar. The reason why the strongest interaction seen with the ωB97XD is not Lys425, as was in PM6-DH+ optimized structure, is because the change in interaction distance of Lys425 in Table 4.1. The elongation in interaction distance by 0.16 Å between PM6-DH+ to ωB97XD methods caused the interaction energy of Lys425 to decrease in the ωB97XD method.

As expected by looking at the interaction distance table, with ωB97XD optimized structure the interaction energy of His362 increased with decreasing interaction distance. Another distance that changes with this optimization method is W1-TPT, an elongation is seen with the magnitude of 1.22 Å compared to PM6-DH+ optimized structure. Without any calculations, the expected result is to observe a decrease in all the residue interactions water bridging with W1. One of such residues is Lys532, and we see interaction energy decrease with ωB97XD method by 3.70 kcal/mol, because the preexisting water bridge between TPT and Lys532 is disrupted. The second residue interacting with TPT through W1 is PTyr723. However, when we look at the interaction energies of two methods we see an increase in interaction energy with ωB97XD method where a decrease is expected.

Considering all the interaction energies calculated with M06-2X and ωB97XD single point calculations with different optimization methods we can say that these results are in agreement with the work of Pan *et al.* which reported that the strongest interaction is observed for Asp533, then Lys425 and Arg364 respectively. The order of the second and third strongest interaction varies with different functional and optimization method but it is to be expected since Pan *et al.* reported the interaction energies with deviations, especially for Asp533 with a deviation in the order of 5.24 kcal/mol. In gas phase calculations increase in the interaction energies was observed. This result is expected since gas phase presents the purely electrostatic interactions. In the PCM corrected water medium we see the lowest interaction energies this too is expected because of polarization. However, the overall interaction energies are too low to be compared to any reference. That is why from here on calculations in water and gas phase will not be considered.

4.3.2. **TPT-Water to Residue interactions**

The interaction energy (ΔE_{INT}) calculation, is carried out with the supramolecular method:

$$\Delta E_{INT} = E_{R-W-TPT} - E_{TPT-W} - E_R \quad (4.20)$$

ΔE_{INT} calculated with above equation treats the water molecules as a part of TPT. Where $E_{R-W-TPT}$ is the single point energy of the residue, bridging water and TPT complex. E_{TPT-W} and E_R is the single point energy of bridging water-TPT complex and residue respectively. This calculation method will only yield different interaction energies for water bridging residues namely PTyr723, Asn722, Thr718, His 632 and Lys532. The other residues will present the same interaction energies as before so they are not presented in Table 4.4.

Table 4.4. Interaction energies (kcal/mol) of residues with water as part of TPT.

	M06-2X[a]//PM6-DH+ (Ɛ=4)	ωB97XD[a]//PM6-DH+ (Ɛ=4)
PTyr723	2.62	-2.11
Asn722	-0.88	-5.27
Thr718	-5.74	-10.00
His632	1.95	-1.46
Lys532	-11.76	-17.34
	M06-2X[a]//ωB97XD	ωB97XD[a]//ωB97XD
PTyr723	-6.21	-6.01
Asn722	-5.66	-5.85
Thr718	-8.31	-8.89
His632	-6.30	-6.46
Lys532	-11.18	-12.49

[a] PCM correction in protein (Ɛ=4)

With the use of this method we achieved only one repulsive interaction which is disadvantageous for the stability of the active site. However, a drawback is that indirect hydrogen bonds such as with Thr718 (-10 kcal/mol) became comparable to the direct hydrogen bonding interactions such as with Lys425 (-11.6 kcal/mol) with PM6-DH+ method. An unexpected result is observed in interaction energies for Thr718. When water is calculated as part of TPT, the interaction of Thr718 is stronger for PM6-DH+ optimized

method. However, the expected result is to be stronger interaction energy for ωB97XD optimized structure, where there is a direct hydrogen bond between TPT and Thr718 besides the water bridge. This result is rationalized when we look back at Figure 4.6. With the PM6-DH+, water (W2) is much more closer to the Thr718 residue compared to ωB97XD, 1.66 Å and 1.78 Å respectively. Even the direct hydrogen bond cannot compensate for the interaction loss for the increase in distance between Thr718 and water. It can be said that this interaction energy calculation method is unsuitable for Thr718. For His632 residue an expected increase in interaction energy is observed for ωB97XD where the Water (W2) and residue distance (1.88 Å) is smaller than PM6-DH+ (2.50 Å). The interaction energy is almost the same between the two methods for Asn722 since the interaction distance between water (W3) and Asn722 is almost the same. The strongest interaction with this method Lys532 is not surprising at all. Lys532 has a direct hydrogen bond and a water bridge contact with TPT, when the water (W1) is expressed as a part of TPT, since the interaction distance is small between water and Lys532 it becomes the strongest interaction. However, this is not realistic since the water-TPT distance is very large (3.08 Å) with ωB97XD, hence water cannot be taken as a part of TPT for calculations of Lys532. This case is also the same for PTyr723 interaction. Since again the water molecule (W1) and TPT distance is very large with ωB97XD, the interaction energy is exaggerated (-6.01 kcal/mol). While PM6-DH+ optimized results are more reliable because water-TPT distance is smaller (1.86 Å) than ωB97XD method.

4.3.3. **TPT to Residue-Water interactions**

The interaction energy (ΔE_{INT}) calculation, is carried out with the supramolecular method:

$$\Delta E_{INT} = E_{R-W-TPT} - E_{TPT} - E_{R-W} \quad (4.3)$$

ΔE_{INT} calculated with the above equation treats the water molecules as a part of residues. Here $E_{R\text{-}W\text{-}TPT}$ is the energy of the residue, bridging water and TPT complex. E_{TPT} and $E_{R\text{-}W}$ is the energy of TPT and residue-water complex respectively. This calculation method will only yield different interaction energies for water bridging residues namely PTyr723, Asn722, Thr718, His 632 and Lys532.

Regarding all the interaction energy calculations so far we can compare the performance of M06-2X and ωB97XD functionals. The most distinct difference between the two is the expression of long-range interaction energies. As expected, ωB97XD functional is better in expressing long range interactions, since it is a long-range corrected functional. However, when short range interactions are considered it is less reliable than M06-2X functional. Computational time for ωB97XD is much more favorable than M06-2X justifying the fact that the interaction energies are based on this functional.

Table 4.5. Interaction energies (kcal/mol) with water calculated as a part of residues.

	M06-2X[a]//PM6-DH+ (Ɛ=4)	ωB97XD[a]//PM6-DH+ (Ɛ=4)
PTyr723	2.56	0.82
Asn722	-2.21	-3.97
Thr718	-5.31	-7.81
His632	-1.94	-3.83
Lys532	-5.63	-8.16
	M06-2X[a]//ωB97XD	ωB97XD[a]//ωB97XD
PTyr723	0.08	-0.12
Asn722	-6.41	-6.74
Thr718	-7.26	-7.21
His632	-4.17	-3.99
Lys532	-1.82	-2.61

[a] PCM correction in protein (Ɛ=4)

When water molecules are expressed as part of residues repulsive interactions are observed for PTyr723 residue. While this result is not desired, with the use of ωB97XD//ωB97XD method a slightly favorable interaction is seen as -0.12 kcal/mol. The interaction energy of Asn722 is increased when compared to the method used in part 4.3.2 while Thr718 it decreased as expected. For His632 an acceptable interaction energy value for a water bridging residue is observed for ωB97XD optimization while in part 4.3.2 the opposite case was observed. The most notable change in interaction energy is seen for Lys532 with the ωB97XD//ωB97XD method. In part 4.3.2 the calculated energy was the strongest (-12.46 kcal/mol), while water is considered as a part of the residue it is -2.61 kcal/mol. This huge difference between two energies are directly related to the water (W1)

and TPT distance as discussed before. This outcome is understandable for ωB97XD method but it is perplexing to see a similar difference in energy for PM6-DH+ method where the water-TPT distance is very close to water-residue one.

After expressing the interaction energies with three methods the main problem is finding out which interaction energy is correct for a water-bridging residue. We can find out the correct result by looking at the water-residue distances and TPT-water distances expressed with three different methods and comparing them with MD results.

Table 4.6.Interaction distances (Å) with PM6-DH+ (Ɛ=4) and ωB97XD/6-31G(d) compared to MD (3 ns).

	MD		PM6-DH+ (Ɛ=4)		ωB97XD	
	W-R	TPT-W	W-R	TPT-W	W-R	TPT-W
PTyr723	1.87	1.97	1.74	1.86	1.76	3.08
Asn722	2.35	1.72	1.83	1.89	1.86	1.88
Thr718	1.86	1.78	1.66	1.76	1.78	2.10
His632	2.85	1.78	2.50	1.88	1.88	2.10
Lys532	1.73	1.97	1.71	1.86	1.70	3.08

From Table 4.6 we draw several conclusions. First of all, there is an apparent increase in the TPT- water (TPT-W) and water-residue (W-R) distances shortened with the ωB97XD optimization. Meaning that water molecules are closer to residues and further away from TPT with this method. While water residue distances are almost same between all the considered amino acid residues. This indicates that the position of water in the active site is determined by the residue-water interactions, and that all the residues interact with water in the same manner. The presence of charged and uncharged residues makes this conclusion inadvisable.

From Table 4.6 it can be inferred whether the water can be taken into account as part of protein or as a part of TPT. If the distance between the water-TPT is smaller than water-protein distance, the interaction energy method in part 4.3.2 will be used. In other words, water will be taken as a part of TPT. Similarly, if the water-TPT distance is smaller than water-protein one, the method in part 4.3.1 will be used. Looking at MD distances, PTyr723 and Lys532 appears to have smaller water-residue interaction distances and hence the water

should be taken into account as a part of the residue. For residues Asn722, Thr718 and His632 the water-TPT distance is smaller than water-residue ones and water molecule should be calculated as part of TPT. Comparing optimization methods with the MD results we see outliers with this deduction. For PM6-DH+, Asn722 and Thr718 have smaller water-residue distances than MD results. However the interaction distances for W-TPT and W-R are very close to each other and the error should be insignificant. When we look at ωB97XD optimization results the outlier interactions increase to three with considerable deviations in distances. This is why several exceptions will be made and in the light of these findings, the interaction energy can be summarized in the following Table 4.7.

Table 4.7.Interaction energies (kcal/mol) comparison with literature.

	ωB97XD[a]//PM6-DH+ (Ɛ=4)	ωB97XD[a]//ωB97XD	MM/GBSA[c]	MD[d]
PTyr723	+0.82	-0.12	-	+1
Asn722	-3.97	-5.85	-	-1
Arg364	-7.84	-6.64	-6.74±1.64	-5
Thr718	-7.81	-7.21	-	-
Lys425	-11.60	-8.20	-6.52±2.26	-
His632	-1.46	-3.99	-	-1
Asp533	-5.94	-8.46	-10.52±5.24	-13
Lys532	-8.16	-1.19[b]	-	-11

[a] PCM correction in protein (Ɛ=4)
[b]Exception
[c]Data from Ref [54]
[d]Data from Fatih University

There is one exception in the final interaction energies calculated with ωB97XD method which is for Lys532. In PM6-DH+ Lys532 maintains a water bridge (W1) interaction with TPT while also interacting without the water bridge as observed in Figure 4.6. However, in ωB97XD optimization the water bridge connecting Lys532 to TPT is disrupted. The method in part 4.3.2 could be used to compensate for the decrease in interaction energy with the disruption of water bridge. However this method would make the interaction of Lys532 in the order of -12.49 kcal/mol. This results would not be feasible at all since Lys425 has smaller interaction distance than Lys532 and has -8.20 kcal/mol interaction energy. The expected result would be to find the interaction of Lys425 stronger than that of Lys532.

When the optimization results are compared with the findings in the literature, ωB97XD method reflects similar results with MM/GBSA calculated results from the work of *Pan et al*. And PM6-DH+ optimization results are similar to the interaction obtained from the MD results by the Fatih University. While, ωB97XD method is more expensive compared to semi-empirical methods, and better presents the results obtained in the work of Pan et al. their MD results were obtained from 10 ns long optimizations, while in this work structures taken from 3 ns MD optimization was used. This means that even taking the initial structure from 3 ns MD, we can achieve similar results obtained from a 10 ns MD. Also PM6-DH+ can be used when the MD optimizations are long and reliable and inexpensive method is desired for the calculation of interaction energies.

4.4. Interaction Energy Calculations for DNA

The interaction contribution DNA could only be calculated by PM6-DH+//PM6-DH+ method in protein phase. The expected result was that the π-π stacking interaction between DNA and TPT should be greater than protein-TPT interactions as reported by Song *et al*.

The interaction energy (ΔE_{INT}) calculation, is carried out with the supramolecular method:

$$\Delta E_{INT} = E_{AA-DNA-TPT} - E_{TPT} - E_{AA-DNA} \quad (4.4)$$

where $E_{AA\text{-}DNA\text{-}TPT}$ is the single point energy for all the residue, DNA and TPT complex. In other words, the energy of the selected active site. E_{TPT} and is the single point energy of TPT while $E_{AA\text{-}DNA}$ is the energy of and DNA and all amino acids. With this equation, the interaction of the whole active site with TPT is calculated.

$$\Delta E_{INT} = E_{DNA-TPT} - E_{TPT} - E_{DNA} \quad (4.5)$$

Equation 4.23 is for the calculation of the interaction energy (ΔE_{INT}) between DNA and TPT. Where $E_{DNA\text{-}TPT}$ is the single point energy for DNA and TPT complex. E_{TPT} and is the single point energy of TPT while E_{DNA} is the energy of DNA.

$$\Delta E_{INT} = E_{AA-TPT} - E_{TPT} - E_{AA} \quad (4.6)$$

Finally, for the interaction energy (ΔE_{INT}) between all the amino acids (AA) and TPT is calculated with the use of equation 4.24. Where $E_{AA\text{-}TPT}$ is the single point energy for all the amino acid residues and TPT complex. E_{TPT} and is the single point energy of TPT while E_{AA} is the energy of amino acids. The resulting calculated interaction energies are presented in Table 4.8.

Table 4.8.Calculated interaction energies (kcal/mol) of the active site (AA-DNA), DNA and all amino acids (AA) with TPT.

	PM6-DH+[a]//PM6-DH+ (Ɛ=4)
AA-DNA	-95.81
DNA	-32.20
AA	-35.94

[a] PCM correction in protein (Ɛ=4)

The whole interaction of the selected active site, meaning that residues and DNA, was calculated and found to be -95.81 kcal/mol. The contribution of DNA to the interaction energy is calculated to be -32.20 kcal/mol, slightly lower that of all amino acid contribution (AA) which calculated to be -35.94 kcal/mol. This reflects the opposite results from the work of Song *et al*. The reasoning behind the similar DNA and amino acid interactions may be reflecting the stability of the cleavage complex. Since neither interaction is dominating, TPT cannot bind to DNA or the enzyme alone. But before any final deductions can be made, calculations should be repeated with a more expensive method such as ωB97XD.

5. CONCLUSION

The findings of the present study provide an insight on the important residues playing a role on the inhibition of Top-DNA cleavage complex in the presence of TPT. The interaction energies of these residues are reported, can be taken into consideration for new Top1-DNA targeting anti-cancer drug development. The quantum chemical interaction energy results were in accordance with the previous molecular dynamics studies.

This work provides a comparison between semi-empirical and DFT methods. For interaction energy calculations semi-empirical method PM6-DH+ can be used as an inexpensive and reliable method if the initial structure is taken from a long molecular dynamics simulation.

The contribution of DNA to interaction energy is calculated similar to all the amino acid residues combined.

6. SUGGESTIONS FOR FUTURE WORK

Interaction energies for carboxylate form of TPT can be investigated in order to address the inactivity problem of this open form. Top1 mutations performed in the work of Pan *et al.* can be investigated for a more comprehensive understanding on interaction between enzyme and TPT.

Optimization with ωB97XD method in protein phase can be conducted to better compare the performance with the PM6-DH+ method.

DNA interactions can be investigated with the use of more expensive methods instead of semi-empirical method for a more comprehensive understanding on DNA and enzyme interaction comparison.

The initial structure used for quantum mechanical calculations can be taken from longer molecular MD simulations for a more realistic result. It is shown that average TPT-residue distances or active site residues can change as presented in Appendix A. A more realistic model can be examined if the initial structure selected for QM calculations are taken from longer MD simulation.

Another approach can be to study the binding energies of other Top1 inhibitor such as Irrinotecan. Exploring TPT like structures can lead to better understanding of active site and design of better anti-cancer agents.

APPENDIX A: MOLECULAR DYNAMICS RESULTS 3NS AND AVG.

Molecular Dynamics calculations were performed using the CHARMM force field [65]. Canonical conditions (NVT) were imposed via the Nose-Hoover thermostat [66,67], and 2 fs time steps are taken employing the SHAKE algorithm [68]. The non-bonded interactions are shifted to zero over 8-12 Å. The ternary complex model of DNA-human Top1-TPT was set up using the protein databank crystal structure 1K4T [16]. The system is immersed into a 60 Å radius sphere of TIP3P [69] water molecules, and charge neutralization was performed by changing waters with sodium ions, where water oxygens had highest electrostatic energies. The system was minimized (within the TIP3P spherical water box) until a root-mean-square gradient of 10-2 kcal/mole, as a result of 1500 steepest descent followed by 1700 steps of adopted basis Newton-Raphson procedure. Then, each system was equilibrated for about 500 ps with the stochastic boundary potential [70] to keep the outmost water molecules. Intel-Xeon-5365 and Intel-Xeon-5462 CPUs are used, employing 8 cores in parallel. The production level simulation is 3 ns long, and has approximately 114.000 atoms.

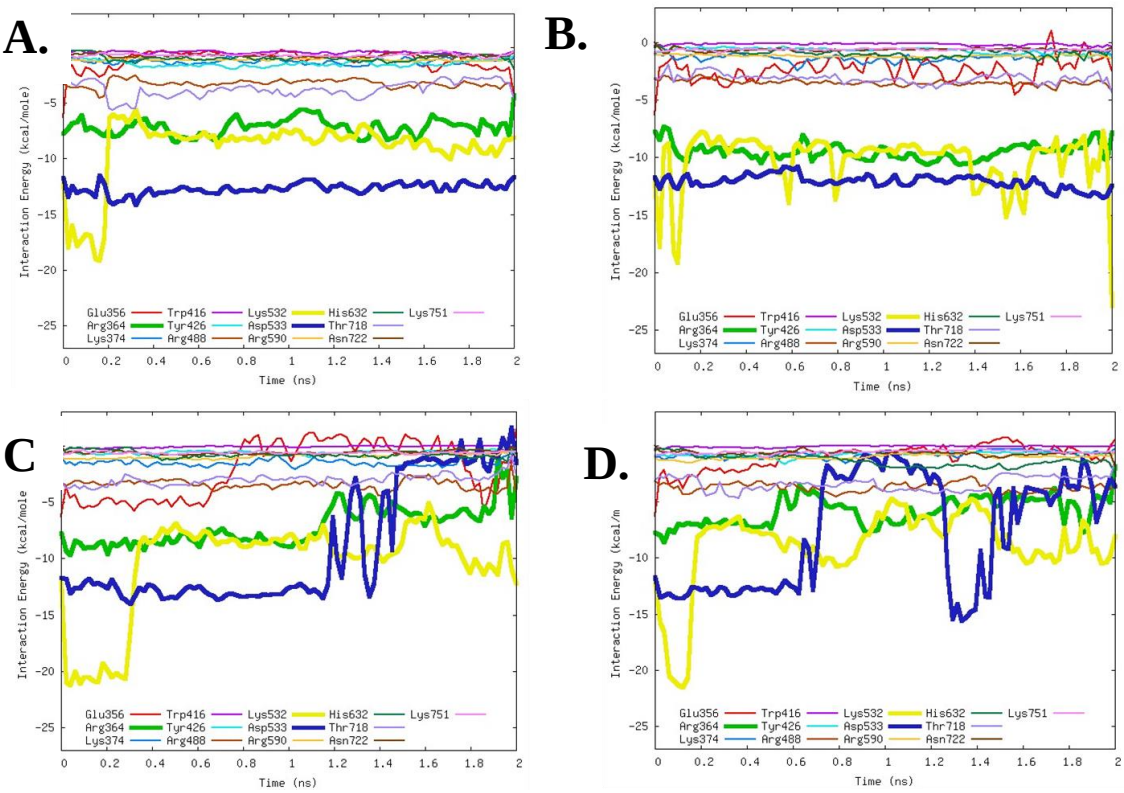

Figure 6.1. Changes in the interaction energy between TPT and residues when (A) 100 pN (B) 200 pN (C) 300 pN (D) 400 pN is applied to the enzyme after 3ns molecular dynamics simulation.

In order to understand the interaction TPT with molecular dynamics approach, different forces were applied to the lip region of the enzyme. Change in the interaction energies were observed in Figure 6.1. These results show that Asp533 residue (blue line) how the highest contribution the interaction energy with TPT. The duration of Asp533 interaction is also stronger than the others as it remains unchanged around 12 kcal/mol when 100 pN and 200 pN force is applied to the enzyme (Figure 6.1.A-B). When the force is increased to 300 pN and 400 pN (Figure 6.1.C-D) we observe that the interaction is broken around 1 ns. Another strong interaction is with Arg364 residue (green line) that is around -7.5 kcal/mol and remain intact until 300 pN force is applied. Moreover, Lys532 residue (yellow line) shows an interaction almost as strong as Asp533 but even with the smallest force 100 pN we observe the interaction starting to decrease 0.2 ns (Figure 6.1.A). We conclude from these findings that over the inspected residues with MD namely: Glu356, Arg364, Lys374, Trp416,

Lys532, Asp533, Arg590, His632, Thr718, Asn722, and Lys751 strongest interactions are seen for Asp533, Lys532 and Arg364 respectively. Comparing these results with the work of Pan *et al.*[54] we see that our results have higher interaction energy. Since in their work they did not calculate the interaction of Lys532 instead calculated Lys425, and in our MD results we did not include Lys425 in the upcoming quantum mechanical calculation the interaction of Lys425 will be addressed.

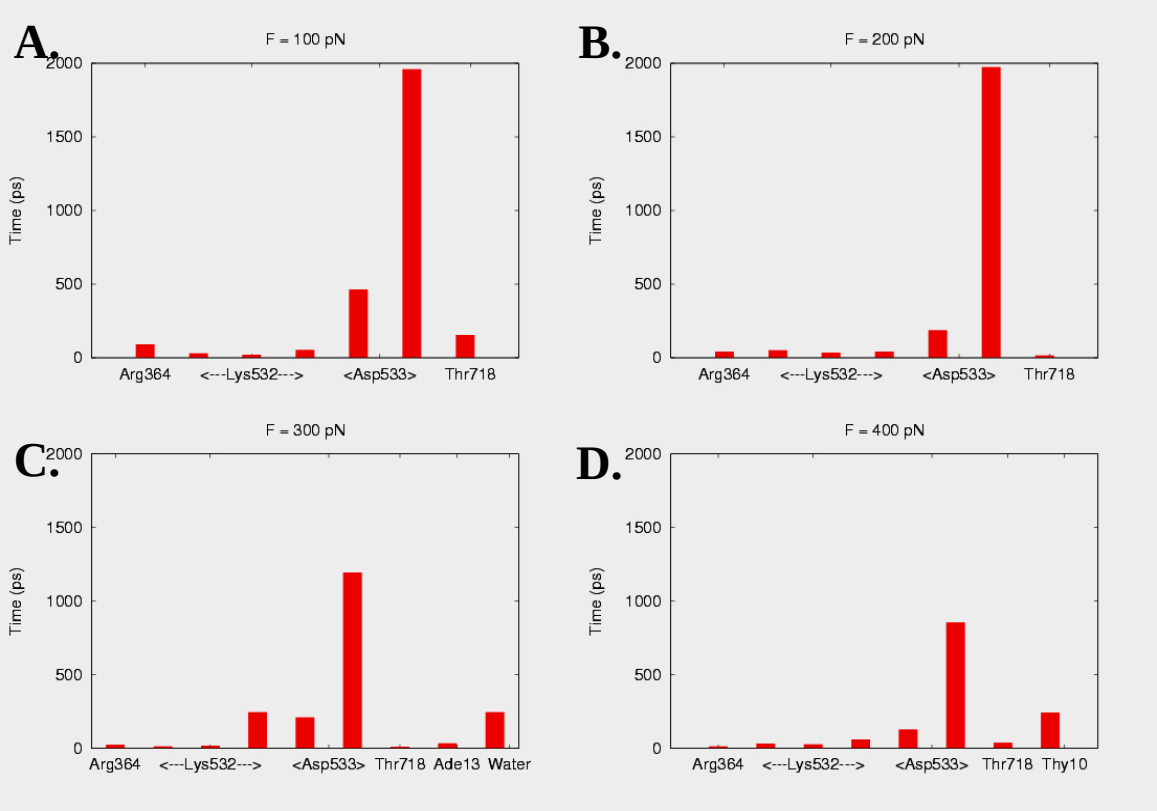

Figure 6.2. Durations of hydrogen-bonding interactions with TPT under (A) 100 pN (B) 200 pN (C) 300 pN (D) 400 pN applied forces.

As seen from Figure 6.2.A-B when the applied force is 100-200 pN the interaction between TPT and Asp533 residue remains intact all through the simulation time (3ns). When the force applied is increased to 300 pN the interaction decreases to 1200 ps and to 400 pN only 950 ps long. This information points out that when force is applied to separate the enzyme from TPT, the interaction with Asp533 severs. Hence the data obtained from MD simulations all point out that interaction of enzyme with TPT in fact prevent the enzyme from leaving. This finding is in accordance with the findings in the 2007 Nature paper [41] which indicated that Top1 targeting anticancer drugs prevents the religation step from occurring.

In this work, we have performed quantum mechanical calculations, initial structure taken from 3 ns long molecular dynamic simulations. It is possible to compare the structure taken from 3 ns simulation with the 10 ns average distances. This will provide us with the answers of two important questions: if it is realistic to start the quantum mechanical calculations from a structure taken from 3 ns long MD really. And, if the interactions seen in this structure are, in fact stable. Some interactions might be brief and not be preserved in a 10 ns long MD. One of such examples are water molecules, bridging hydrogen bond interactions between TPT and the enzyme. One molecule of water is rarely stationary, even in the presence of a stabilizing interactions. The disruption of such interactions can easily be observed, to be replaced by another water molecule in the course of the MD. However, being not able to track the changes of distance between water and enzyme is not important, since it is possible to do so for each amino acid residue and TPT distances.

Table 6.1. Calculated interaction distances (Å) between TPT and residues for 3 ns and average (avg.) of 10 ns MD.

	3 ns MD	Avg. 10 ns MD
PTyr723	7.2	6.5
Asn722	5.7	6.3
Arg364	3.9	3.8
Thr718	3.4	3.3
Lys425	2.7	3.7
His632	5.6	6.3
Asp533	2.9	3.8
Lys532	5.6	6.3
Glu356	8.3	5.7

In Table 6.1 the 3 ns and average 10 ns residue-TPT distances are presented. For the quantum mechanical calculations the selected active site from 3 ns MD was constructed from the residues within 8 Å radius away from TPT. Glu356 residue were not counted in the calculations carried out in this study. However, when we see the distance between Glu356 and TPT is shortened in average 10 ns MD distances. It is obvious that in average 10 ns MD simulation the interaction of this residue is stronger than in 3 ns. The other residues are all considered, but for most residues longer interaction distances are observed. Some remain almost unchanged such as Arg364 and Thr718.

REFERENCES

1. Champoux, J.J., "DNA TOPOISOMERASES : Structure , Function , And Mechanism", *Annual Review Biochemistry*, pp. 369–413, 2001.

2. Wang, J.C., "Cellular Roles Of DNA Topoisomerases: A Molecular Perspective", *Nature reviews. Molecular Cell Biology*, Vol. 3, pp. 430–440, 2002.

3. Corbett, K.D., and J.M. Berger, "Structure, Molecular Mechanisms, And Evolutionary Relationships In DNA Topoisomerases", *Annual Review of Biophysics and Biomolecular Structure*, Vol. 33, pp. 95–118, 2004.

4. Di Nunzio, M.R., Y. Wang, and A. Douhal, "Structural Photodynamic Behavior Of Topotecan, A Potent Anticancer Drug, In Aqueous Solutions At Different PHs", *Journal of Physical Chemistry B*, Vol. 116, pp. 8182–8190, 2012.

5. Hsiang, Y.H., R. Hertzberg, S. Hecht, and L.F. Liu, "Camptothecin Induced Protein-linked DNA Breaks Via Mammalian DNA Topoisomerase", *Journal of Biological Chemistry*, Vol. 260, pp. 14873–14878, 1985.

6. Been, M.D., and J.J. Champoux, "Breakage Of Single-stranded DNA By Eukaryotic Type 1 Topoisomerase Occurs Only At Regions With The Potential For Base-pairing", *Journal of Molecular Biology*, Vol. 180, pp. 515–531, 2015.

7. Stewart, L., G.C. Ireton, and J.J. Champoux, "The Domain Organization Of Human Topoisomerase I", *The Journal of Biological Chemistry*, Vol. 271, pp. 7602–7608, 1996.

8. Redinbo, M.R., L. Stewart, P. Kuhn, J.J. Champoux, and W.G. Hol, "Crystal Structures Of Human Topoisomerase I In Covalent And Noncovalent Complexes With DNA", *Science (New York, N.Y.)*, Vol. 279, pp. 1504–1513, 1998.

9. Stewart, L., M.R. Redinbo, X. Qiu, W.G. Hol, and J.J. Champoux, "A Model For The Mechanism Of Human Topoisomerase I", *Science (New York, N.Y.)*, Vol. 279, pp. 1534–1541, 1998.

10. Tse, Y.C., K. Kirkegaard, and J.C. Wang, "Covalent Bonds Between Protein And DNA. Formation Of Phosphotyrosine Linkage Between Certain DNA Topoisomerases And DNA", *Journal of Biological Chemistry*, Vol. 255, pp. 5560–5565, 1980.

11. Holden, J. a, M.E. Wall, M.C. Wani, and G. Manikumar, "Human DNA Topoisomerase I: Quantitative Analysis Of The Effects Of Camptothecin Analogs And The Benzophenanthridine Alkaloids Nitidine And 6-ethoxydihydronitidine On DNA Topoisomerase I-induced DNA Strand Breakage", *Archives of biochemistry and biophysics*, Vol. 370, pp. 66–76, 1999.

12. Pommier, Y., "Topoisomerase I Inhibitors: Camptothecins And Beyond", *Nature Reviews Cancer*, Vol. 6, pp. 789–802, 2006.

13. Hsiang, Y., and L.F. Liu, "Identification Of Mammalian DNA Topoisomerase I As An Intracellular Target Of The Anticancer Drug Camptothecin Identification Of Mammalian DNA Topoisomerase I As An Intracellular Target Of The Anticancer Drug Camptothecin1", *Cancer Research*, Vol. 48, pp. 1722–1726, 1988.

14. Pommier, Y., G. Kohlhagen, K.W. Kohn, F. Leteurtre, M.C. Wani, and M.E. Wall, "Interaction Of An Alkylating Camptothecin Derivative With A DNA Base At Topoisomerase I-DNA Cleavage Sites", *Proceedings of the National Academy of Sciences of the United States of America*, Vol. 92, pp. 8861–8865, 1995.

15. Kepler, J., "Plant Antitumor Agents. IV. An Approach Toward The Synthesis Of Camptothecin", *The Journal of Organic Chemistry*, Vol. 34, pp. 3853–3858, 1969.

16. Staker, B.L., K. Hjerrild, M.D. Feese, C. a Behnke, A.B. Burgin, and L. Stewart, "The Mechanism Of Topoisomerase I Poisoning By A Camptothecin Analog", *Proceedings of the National Academy of Sciences of the United States of America*, Vol. 99, pp. 15387–15392, 2002.

17. Wang, J.C., "DNA Topoisomerases", *Annual Review Biochemistry*, Vol. 65, pp. 635–692, 1996.

18. Hertzberg, R.P., M.J. Caranfa, and S.M. Hecht, "On The Mechanism Of Topoisomerase I Inhibition By Camptothecin: Evidence For Binding To An Enzyme-DNA Complex", *Biochemistry*, Vol. 28, pp. 4629–4638, 1989.

19. Eng, W.K., L. Faucette, R.K. Johnson, and R. Sternglanz, "Evidence That DNA Topoisomerase I Is Necessary For The Cytotoxic Effects Of Camptothecin", *Molecular pharmacology*, Vol. 34, pp. 755–760, 1988.

20. Madden, K.R., and J.J. Champoux, "Overexpression Of Human Topoisomerase I In Baby Hamster Kidney Cells : Hypersensitivity Of Clonal Isolates To Camptothecin Overexpression Of Human Topoisomerase I In Baby Hamster Kidney Cells: Hypersensitivity Of Clonal Isolates To Camptothecin", *Cancer research*, Vol. 52(3), pp. 525–532, 1992.

21. Hann, C., D.L. Evans, J. Fertala, P. Benedetti, M.A. Bjornsti, and D.J. Hall, "Increased Camptothecin Toxicity Induced In Mammalian Cells Expressing Saccharomyces Cerevisiae DNA Topoisomerase I", *Journal of Biological Chemistry*, Vol. 273, pp. 8425–8433, 1998.

22. Chrencik, J.E., B.L. Staker, A.B. Burgin, P. Pourquier, Y. Pommier, L. Stewart, and M.R. Redinbo, "Mechanisms Of Camptothecin Resistance By Human Topoisomerase I Mutations", *Journal of Molecular Biology*, Vol. 339, pp. 773–784, 2004.

23. Minsky, B.D., "Combined-modality Therapy Of Rectal Cancer With Irinotecan-based Regimens", *Oncology (Williston Park, N.Y.)*, Vol. 18, pp. 49–55, 2004.

24. Rodriguez-Galindo, C., K. Radomski, C.F. Stewart, W. Furman, V.M. Santana, and P.J. Houghton, "Clinical Use Of Topoisomerase I Inhibitors In Anticancer Treatment", *Medical and Pediatric Oncology*, Vol. 35, pp. 385–402, 2000.

25. Stewart, D.J., "Topotecan In The First-line Treatment Of Small Cell Lung Cancer", *The Oncologist*, Vol. 9, pp. 33–42, 2004.

26. Koster, D. a., F. Czerwinski, L. Halby, A. Crut, P. Vekhoff, K. Palle, P.B. Arimondo, and N.H. Dekker, "Single-molecule Observations Of Topotecan-mediated TopIB

Activity At A Unique DNA Sequence", *Nucleic Acids Research*, Vol. 36, pp. 2301–2310, 2008.

27. Punchihewa, C., M. Carver, and D. Yang, "DNA Sequence Selectivity Of Human Topoisomerase I-mediated DNA Cleavage Induced By Camptothecin", *Protein Science*, Vol. 18, pp. 1326–1331, 2009.

28. Burke, T.G., and Z. Mi, "The Structural Basis Of Camptothecin Interactions With Human Serum Albumin: Impact On Drug Stability", *Journal of Medicinal Chemistry*, Vol. 37, pp. 40–46, 1994.

29. Schellens, J.H., G.J. Creemers, J.H. Beijnen, H. Rosing, M. de Boer-Dennert, M. McDonald, B. Davies, and J. Verweij, "Bioavailability And Pharmacokinetics Of Oral Topotecan: A New Topoisomerase I Inhibitor", *British Journal of Cancer*, Vol. 73, pp. 1268–1271, 1996.

30. Ewesuedo, R., and M. Ratain, "Topoisomerase I Inhibitors", *The Oncologist*, Vol. 2, pp. 359–364, 1997.

31. Bailly, C., "Homocamptothecins: Potent Topoisomerase I Inhibitors And Promising Anticancer Drugs", *Critical Reviews in Oncology/Hematology*, Vol. 45, pp. 91–108, 2003.

32. Underberg, W.J.M., R.M.J. Goossen, B.R. Smith, and J.H. Beijnen, "Equilibrium Kinetics Of The New Experimental Anti-tumour Compound SK&F 104864-A In Aqueous Solution", *Journal of Pharmaceutical and Biomedical Analysis*, Vol. 8, pp. 681–683, 2015.

33. Fassberg, J., and V. Stella, "A Kinetic And Mechanistic Study Of The Hydrolysis Of Camptothecin And Some Analogues", *Journal of Pharmaceutical Sciences*, Vol. 81, pp. 676-684, 1992.

34. Yao, S., D. Murali, P. Seetharamulu, K. Haridas, P.N. V Petluru, D.G. Reddy, and F.H. Hausheer, "Topotecan Lactone Selectively Binds To Double- And Single-stranded DNA In The Absence Of Topoisomerase I", *Cancer Research*, Vol. 58, pp. 3782–3786, 1998.

35. Warner, D.L., and T.G. Burke, “Simple And Versatile High-performance Liquid Chromatographic Method For The Simultaneous Quantitation Of The Lactone And Carboxylate Forms Of Camptothecin Anticancer Drugs”, *Journal of Chromatography B: Biomedical Applications*, Vol. 691, pp. 161–171, 1997.

36. Gallo, J.M., P.B. Laub, E.K. Rowinsky, L.B. Grochow, and S.D. Baker, “Population Pharmacokinetic Model For Topotecan Derived From Phase I Clinical Trials”, *Journal of clinical oncology : official journal of the American Society of Clinical Oncology*, Vol. 18, pp. 2459–67, 2000.

37. Mcclay, E.F., “Cancer Management in Man: Chemotherapy, Biological Therapy, Hyperthermia and Supporting Measures”, *Cancer Management in Man: Chemotherapy, Biological Therapy, Hyperthermia and Supporting Measures*, 2011.

38. Adams, D.J., M.W. Dewhirst, J.L. Flowers, M.P. Gamcsik, O.M. Colvin, G. Manikumar, M.C. Wani, and M.E. Wall, “Camptothecin Analogues With Enhanced Antitumor Activity At Acidic PH”, *Cancer Chemotherapy and Pharmacology*, Vol. 46, pp. 263–271, 2000.

39. Yang, D., J. Thompson Strode, H. Peter Spielmann, a. H.J. Wang, and T.G. Burke, “Dna Interactions Of Two Clinical Camptothecin Drugs Stabilize Their Active Lactone Forms”, *Journal of the American Chemical Society*, Vol. 120, pp. 2979–2980, 1998.

40. Thomas, C.J., N.J. Rahier, and S.M. Hecht, “Camptothecin: Current Perspectives”, *Bioorganic and Medicinal Chemistry*, Vol. 12, pp. 1585–1604, 2004.

41. Koster, D. a, K. Palle, E.S.M. Bot, M.-A. Bjornsti, and N.H. Dekker, “Antitumour Drugs Impede DNA Uncoiling By Topoisomerase I”, *Nature*, Vol. 448, pp. 213–217, 2007.

42. Fiorani, P., J.F. Amatruda, a Silvestri, R.H. Butler, M. a Bjornsti, and P. Benedetti, “Domain Interactions Affecting Human DNA Topoisomerase I Catalysis And Camptothecin Sensitivity”, *Molecular Pharmacology*, Vol. 56, pp. 1105–1115, 1999.

43. Mancini, G., I. D’Annessa, A. Coletta, N. Sanna, G. Chillemi, and A. Desideri, “Structural And Dynamical Effects Induced By The Anticancer Drug Topotecan On The Human Topoisomerase I - DNA Complex”, *Plos One*, Vol. 5, pp. 1-10, 2010.

44. Siu, F.-M., and C.-M. Che, "Persistence Of Camptothecin Analog-topoisomerase I-DNA Ternary Complexes: A Molecular Dynamics Study", *Journal of the American Chemical Society*, Vol. 130, pp. 17928–17937, 2008.

45. Fiorani, P., A. Bruselles, M. Falconi, G. Chillemi, A. Desideri, and P. Benedetti, "Single Mutation In The Linker Domain Confers Protein Flexibility And Camptothecin Resistance To Human Topoisomerase I", *Journal of Biological Chemistry*, Vol. 278, pp. 43268–43275, 2003.

46. Chillemi, G., P. Fiorani, S. Castelli, A. Bruselles, P. Benedetti, and A. Desideri, "Effect On DNA Relaxation Of The Single Thr718Ala Mutation In Human Topoisomerase I: A Functional And Molecular Dynamics Study", *Nucleic Acids Research*, Vol. 33, pp. 3339–3350, 2005.

47. Mazzini, S., M.C. Bellucci, S. Dallavalle, F. Fraternali, and R. Mondelli, "Mode Of Binding Of Camptothecins To Double Helix Oligonucleotides", *Organic & Biomolecular Chemistry*, Vol. 2, pp. 505–513, 2004.

48. Miller, S.E., and D.S. Pilch, "A Spectrophotometric Study Of The PH-dependent And DNA Binding Properties Of Topotecan", *Annals of the New York Academy of Sciences*, Vol. 922, pp. 309–313, 2000.

49. Sanna, N., G. Chillemi, A. Grandi, S. Castelli, A. Desideri, and V. Barone, "New Hints On The PH-driven Tautomeric Equilibria Of The Topotecan Anticancer Drug In Aqueous Solutions From An Integrated Spectroscopic And Quantum-mechanical Approach", *Journal of the American Chemical Society*, Vol. 127, pp. 15429–15436, 2005.

50. Fujimori, A., W.G. Harker, G. Kohlhagen, Y. Hoki, and Y. Pommier, "Mutation At The Catalytic Site Of Topoisomerase I In CEM / C2 , A Human Leukemia Cell Line Resistant To Camptothecin", *Cancer Research*, pp. 1339–1346, 1995.

51. Tamura, H., C. Kohchi, R. Yamada, T. Ikeda, O. Koiwai, E. Patterson, J.D. Keene, K. Okada, E. Kjeldsen, and K. Nishikawa, "Molecular Cloning Of A CDNA Of A

Camptothecin-resistant Human DNA Topoisomerase I And Identification Of Mutation Sites", *Nucleic Acids Research*, Vol. 19, pp. 69–75, 1991.

52. Li, X.G., P. Haluska, Y.H. Hsiang, A.K. Bharti, D.W. Kufe, L.F. Liu, and E.H. Rubin, "Involvement Of Amino Acids 361 To 364 Of Human Topoisomerase I In Camptothecin Resistance And Enzyme Catalysis", *Biochemical Pharmacology*, Vol. 53, pp. 1019–1027, 1997.

53. Song, Y., and M. Cushman, "The Binding Orientation Of A Norindenoisoquinoline In The Topoisomerase I-DNA Cleavage Complex Is Primarily Governed By ??-?? Stacking Interactions", *Journal of Physical Chemistry B*, Vol. 112, pp. 9484–9489, 2008.

54. Pan, P., Y. Li, H. Yu, H. Sun, and T. Hou, "Molecular Principle Of Topotecan Resistance By Topoisomerase I Mutations Through Molecular Modeling Approaches", *Journal of Chemical Information and Modelling*, Vol. 53, pp. 997–1006, 2013.

55. Zhao, Y., and D.G. Truhlar, "The M06 Suite Of Density Functionals For Main Group Thermochemistry, Thermochemical Kinetics, Noncovalent Interactions, Excited States, And Transition Elements: Two New Functionals And Systematic Testing Of Four M06-class Functionals And 12 Other Function", *Theoretical Chemistry Accounts*, Vol. 120, pp. 215–241, 2008.

56. Stewart, J.J.P., "Optimization Of Parameters For Semiempirical Methods I. Method", *Journal of Computational Chemistry*, Vol. 10, pp. 209–220, 1989.

57. Stewart, J.J.P., "Optimization Of Parameters For Semiempirical Methods II. Applications", *Journal of Computational Chemistry*, Vol. 10, pp. 155–64, 1989.

58. Stewart, J.J.P., "Optimization Of Parameters For Semiempirical Methods IV: Extension Of MNDO, AM1 And PM3 To More Main Group Elements", *Journal of Molecular Modeling*, Vol. 10, pp. 155–164, 2004.

59. Stewart, J.J.P., "Optimization Of Parameters For Semiempirical Methods V: Modification Of NDDO Approximations And Application To 70 Elements", *Journal of Molecular Modeling*, Vol. 13, pp. 1173–1213, 2007.

60. Becke, A.D., “A New Mixing Of Hartree–Fock And Local Density-functional Theories”, *The Journal of Chemical Physics*, Vol. 98, pp. 1372, 1993.

61. Korth, M., “Third-generation Hydrogen-bonding Corrections For Semiempirical QM Methods And Force Fields”, *Journal of Chemical Theory and Computation*, Vol. 6, pp. 3808–3816, 2010.

62. Stewart, J.J.P., “MOPAC: A Semiempirical Molecular Orbital Program”, *Journal of Computer-Aided Molecular Design*, Vol. 4, pp. 1–103, 1990.

63. Klamt, A., and G. Schuurmann, “COSMO: A New Approach To Dielectric Screening In Solvents With Explicit Expressions For The Screening Energy And Its Gradient”, *Journal of the Chemical Society, Perkin Transactions 2*, pp. 799, 1993.

64. Frisch, M.J., and et. al, “Gaussian09 Revision A.1”, *Gaussian 09, Revision A.02* 2009.

65. Brooks, B.R., R.E. Bruccoleri, B.D. Olafson, D.J. States, S. Swaminathan, and M. Karplus, “CHARMM: A Program For Macromolecular Energy, Minimization, And Dynamics Calculations”, *Journal of Computational Chemistry*, Vol. 4, pp. 187–217, 1983.

66. Nose, S., S. Nosé, and S. Nosé, “A Unified Formulation Of The Constant Temperature Molecular Dynamics Methods”, *The Journal of Chemical Physics*, Vol. 81, pp. 511–519, 1984.

67. Hoover, W.G., “Canonical Dynamics: Equilibrium Phase-space Distributions”, *Physical Review A*, Vol. 31, pp. 1695–1697, 1985.

68. Ryckaert, J.-P., G. Ciccotti, and H.J.. Berendsen, “Numerical Integration Of The Cartesian Equations Of Motion Of A System With Constraints: Molecular Dynamics Of N-alkanes”, *Journal of Computational Physics*, Vol. 23, pp. 327–341, 2014.

69. Jorgensen, W.L., J. Chandrasekhar, J.D. Madura, R.W. Impey, and M.L. Klein, “Comparison Of Simple Potential Functions For Simulating Liquid Water”, *The Journal of Chemical Physics*, Vol. 79, pp. 926-935, 1983.

70. Brooks, C.L., a Brünger, and M. Karplus, “Active Site Dynamics In Protein Molecules: A Stochastic Boundary Molecular-dynamics Approach”, *Biopolymers*, Vol. 24, pp. 843–865, 1985.